The Journal of Chemical Physics

RESEARCH ARTICLE | JANUARY 31 2024

Designer pair statistics of disordered many-particle systems with novel properties

Haina Wang ; Salvatore Torquato

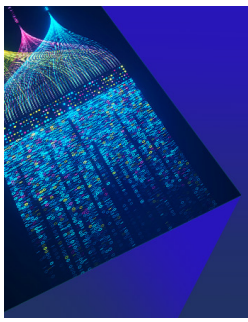
Check for updates

J. Chem. Phys. 160, 044911 (2024)
https://doi.org/10.1063/5.0189769

View Online
Export Citation
CrossMark

31 January 2024 15:02:42

AIP Publishing


Chemical Physics Reviews
Special Topic: AI and Machine Learning in Chemical and Materials Science
Submit Today
AIP Publishing

The Journal of Chemical Physics ARTICLE pubs.aip.org/aip/jcp

Designer pair statistics of disordered many-particle systems with novel properties

Cite as: J. Chem. Phys. 160, 044911 (2024); doi: 10.1063/5.0189769
Submitted: 30 November 2023 • Accepted: 2 January 2024 •
Published Online: 31 January 2024

View Online Export Citation CrossMark

Haina Wang[1] and Salvatore Torquato[2,3,a)]

AFFILIATIONS

[1] Department of Chemistry, Princeton University, Princeton, New Jersey 08544, USA
[2] Department of Chemistry, Department of Physics, Princeton Materials Institute, and Program in Applied and Computational Mathematics, Princeton University, Princeton, New Jersey 08544, USA
[3] School of Natural Sciences, Institute for Advanced Study, 1 Einstein Drive, Princeton, New Jersey 08540, USA

[a)] **Author to whom correspondence should be addressed:** torquato@princeton.edu

ABSTRACT

The knowledge of exact analytical functional forms for the pair correlation function $g_2(r)$ and its corresponding structure factor $S(k)$ of disordered many-particle systems is limited. For fundamental and practical reasons, it is highly desirable to add to the existing database of analytical functional forms for such pair statistics. Here, we design a plethora of such pair functions in direct and Fourier spaces across the first three Euclidean space dimensions that are realizable by diverse many-particle systems with varying degrees of correlated disorder across length scales, spanning a wide spectrum of hyperuniform, typical nonhyperuniform, and antihyperuniform ones. This is accomplished by utilizing an efficient inverse algorithm that determines equilibrium states with up to pair interactions at positive temperatures that precisely match targeted forms for both $g_2(r)$ and $S(k)$. Among other results, we realize an example with the strongest hyperuniform property among known positive-temperature equilibrium states, critical-point systems (implying unusual 1D systems with phase transitions) that are not in the Ising universality class, systems that attain self-similar pair statistics under Fourier transformation, and an experimentally feasible polymer model. We show that our pair functions enable one to achieve many-particle systems with a wide range of translational order and self-diffusion coefficients $\mathcal{D}$, which are inversely related to one another. One can design other realizable pair statistics via linear combinations of our functions or by applying our inverse procedure to other desirable functional forms. Our approach facilitates the inverse design of materials with desirable physical and chemical properties by tuning their pair statistics.

Published under an exclusive license by AIP Publishing. https://doi.org/10.1063/5.0189769

31 January 2024 15:02:42

I. INTRODUCTION

The determination of equilibrium and nonequilibrium properties of disordered many-particle systems in d-dimensional Euclidean space $\mathbb{R}^d$ based on structural information contained in correlation functions is of fundamental and practical importance in statistical and condensed-matter physics, chemistry, mathematics, biological sciences, and materials engineering.[1–8] The pair correlation function $g_2(\mathbf{r})$ and the corresponding structure factor $S(\mathbf{k})$ are widely used structural functions due to their computational simplicity and experimental accessibility through diffraction measurements. They enable one to determine key equilibrium bulk properties, such as the pressure, the isothermal compressibility,[4,7] and the two-body excess entropy.[9] Moreover, pair statistics are crucial inputs for the determination of transport properties of many-particle systems, including Enskog theories for the self-diffusion coefficient[10–12] and the shear and bulk viscosities,[13] as well as the effective temperatures of structural glasses[14] and the time-dependent diffusion spreadability.[15]

Despite the importance of such pair functions in direct and Fourier spaces [i.e., $g_2(\mathbf{r})$ and $S(\mathbf{k})$, respectively], there are only a relatively small number of disordered many-particle systems for which we know exact analytical pair functions over their entire parameter regime. These include determinantal point processes across space dimensions,[1,2,16–21] equilibrium one-dimensional (1D) hard rods,[22] "ghost" random sequential addition (RSA) process across dimensions,[23] and 2D and 3D unit-step function $g_2(\mathbf{r})$ at all densities up to the "terminal packing fraction" $1/2^d$.[24] Given our current limited knowledge of analytical pair functions, it is highly desirable to expand the existing database of radial functional forms of

Published under an exclusive license by AIP Publishing

$g_2(r)$ and $S(k)$ that can be achieved by statistically homogeneous and isotropic disordered many-particle systems, where $r = |\mathbf{r}|$ and $k = |\mathbf{k}|$. Substantially increasing such a database would enable one to probe the space of equilibrium and nonequilibrium properties analytically in comprehensive ways not heretofore possible. Furthermore, adding to such a database would facilitate the inverse design of materials with desirable mechanical, optical, and chemical properties, which could be further accelerated by machine learning techniques.[25]

A hypothesized functional form for the pair correlation function $g_2(r)$ is not necessarily realized by a many-particle system at number density ρ, even if the corresponding structure factor $S(k)$ is nonnegative for all k, as it must be.[19,26,27] This realizability problem has a rich and long history,[19,26–31] but it is a notoriously difficult problem to solve because an uncountable number of necessary and sufficient conditions are generally required,[30,31] which are not possible to check in practice. This complexity places great importance on the need to formulate algorithms to construct particle configurations that realize targeted hypothetical functional forms of the pair statistics.[24,32]

In this work, we design a plethora of exact functional forms for pair correlations in direct and Fourier spaces across the first three Euclidean space dimensions that are realizable by diverse many-particle systems with varying degrees of correlated disorder across length scales with novel structural and physical properties. As suggested by Zhang and Torquato,[32] we solve this realizability problem here by employing an efficient inverse algorithm[33] that determines classical equilibrium states with up to pair interactions $v(r)$ at positive temperature T that precisely match targeted forms for both $g_2(r)$ and $S(k)$. Our methodology minimizes an objective function that incorporates pair statistics in both direct and Fourier spaces so that the small-, intermediate-, and large-distance correlations are very accurately captured; see Sec. II for details.

For purposes of illustration, we consider a broad range of functional forms that span across a wide spectrum of hyperuniform and nonhyperuniform classes. Disordered hyperuniform systems anomalously suppress large-scale density fluctuations compared to typical disordered systems, such as liquids.[34] A point pattern in $\mathbb{R}^d$ is hyperuniform if the local number variance $\sigma^2(R) = \langle N^2(R)\rangle - \langle N(R)\rangle^2$ of the number of points $N(R)$ found in a spherical window of radius R grows slower than R^d in the large-R limit.[34,35] Equivalently, a hyperuniform state is characterized by a structure factor that vanishes in the infinite-wavelength limit, i.e., $\lim_{k\to 0} S(k) = 0$. Often, the structure factor of hyperuniform systems takes a radial power-law form in the vicinity of the origin, i.e., $S(k) \sim k^{\alpha}$, where α is a positive exponent. The value of α determines different large-R scaling behaviors of the number variance,[34–36] i.e.,

$$\sigma^2(R) \sim \begin{cases} R^{d-1}, & \alpha > 1 \text{ (class I)}, \\ R^{d-1} \ln R, & \alpha = 1 \text{ (class II)}, \\ R^{d-\alpha}, & 0 < \alpha < 1 \text{ (class III)}. \end{cases} \tag{1}$$

Disordered hyperuniform systems are exotic states of matter that have been receiving great attention because they connect a variety of seemingly unrelated systems that arise in physics, chemistry, materials science, mathematics, and biology.[35] By contrast, for any *nonhyperuniform* system, the local variance has the following large-R scaling behaviors:[37]

$$\sigma^2(R) \sim \begin{cases} R^{d}, & \alpha = 0 \text{ (typical nonhyperuniform)}, \\ R^{d-\alpha}, & \alpha < 0 \text{ (antihyperuniform)}. \end{cases} \tag{2}$$

For a "typical" nonhyperuniform system, $S(0)$ is bounded. In antihyperuniform systems, $S(0)$ is unbounded, i.e., $\lim_{k\to 0} S(k) = +\infty$, and, hence, they are diametrically opposite to hyperuniform systems. Typical nonhyperuniform states have a bounded nonzero value of $S(k)$ as $k \to 0$.[37] Antihyperuniform systems include those at thermal critical points (e.g., liquid–vapor and magnetic critical points),[38–42] as well as fractals[43] and certain substitution tilings.[44]

Table I lists the target $g_2(r)$ and $S(k)$ functions considered here and shown to be realizable. The hyperuniform pair functions that we target include d-dimensional Gaussians, d-dimensional generalization of the one-component plasma (OCP) and their Fourier duals,[32] d-dimensional hyperbolic secant function $g_2(r)$, and a 2D Gaussian-damped polynomial. The typical nonhyperuniform functions include a 1D Hermite–Gaussian function, a hypothetical 3D hyposurficial state,[34] as well as 1D and 2D ghost RSA packings.[23] These functional forms are chosen for their fundamental significance, their capability to yield systems in which particles form clusters of various sizes, and their potential applications in material design. It is noteworthy that the Gaussian functions, the 1D hyperbolic secant function, the 2D Gaussian-damped polynomial, and the 1D Hermite–Gaussian function have the property that they are self-similar under Fourier transformations. Self-similar pair statistics enable one to exploit duality relations in the phase diagrams of soft-matter systems. For example, via duality relations, information about low-density classical ground states under short-ranged interactions can be mapped to high-density ground states under long-ranged interactions.[45,46] This knowledge facilitates the determination of ground-state structures over large density ranges,[46] which may provide good solutions to *covering* and *quantizer* problems that arise in discrete geometry and have many applications,[47] including wireless communication network layouts.

We also, for the first time, demonstrate the realizability of antihyperuniform systems across the first three space dimensions corresponding to critical points that do not belong to the Ising universality class, including a remarkable 1D critical-point state, which is to be contrasted with typical 1D systems in which phase transitions cannot exist. Note that the pair functions in Table I possess analytical forms in both direct and Fourier spaces in all but two cases: the 2D hyperbolic secant $g_2(r)$ and the 2D ghost RSA packing, for which $g_2(r)$ are known analytically but $S(k)$ must be numerically evaluated to high precision. The reasons for choosing the targets in Table I are detailed in Sec. III.

The functional forms of our pair statistics and their corresponding potentials can be used to model soft-core polymers with varying magnitudes of short- and long-range repulsive forces [Eqs. (3)–(10), (20), (21)], "sticky" macromolecules with oscillatory interactions [Eqs. (16)–(19)], as well as polymer-grafted nanoparticles with both hard- and soft-core interactions [Eqs. (22)–(24)]. Notably, we discover that one of our models possesses a stronger hyperuniform property (i.e., a larger exponent α) than any other positive-temperature equilibrium state known previously. To illustrate that our procedure can be used to guide experimental polymer design,

31 January 2024 15:02:42

Published under an exclusive license by AIP Publishing

TABLE I. Analytical target pair statistics studied here and shown to be realizable by statistically homogeneous and isotropic disordered many-particle systems in various spatial dimensions. The small-k scaling exponents α in Eq. (1) are shown. All states are at $\rho = 1$. The definitions of the special functions and symbols in the pair statistics are given in the table footnotes.

Functional form	d	$g_2(r)$	$S(k)$	α
Gaussian	1, 2, 3	$1-\exp\left(-\pi r^2\right)$ (3)	$1-\exp\left(-\frac{k^2}{4\pi}\right)$ (4)	2
Generalized OCP[48]	3	$1-\exp\left(-\frac{4\pi}{3}r^3\right)$ (5)	$1-{}_1F_4\left(1;\frac{1}{3},\frac{2}{3},\frac{5}{6},\frac{7}{6};-\frac{k^6}{20\,736\pi^2}\right)+\frac{2\pi\mathrm{ber}_{\frac{2}{3}}\left(\frac{(k^2)^{3/4}}{3\sqrt{\pi}}\right)}{3\sqrt{3}}+\frac{2\pi\mathrm{ber}_{-\frac{2}{3}}\left(\frac{(k^2)^{3/4}}{3\sqrt{\pi}}\right)}{3\sqrt{3}}$ (6)	2
Fourier dual of OCP	1	$1-\frac{1}{\pi r^2+1}$ (7)	$1-\exp\left(-k/\pi\right)$ (8)	1
Fourier dual of OCP[48]	3	$1-{}_1F_4\left(1;\frac{1}{3},\frac{2}{3},\frac{5}{6},\frac{7}{6};-\frac{1}{324}\pi^4r^6\right)+\frac{2\pi\mathrm{ber}_{\frac{2}{3}}\left(\frac{2}{3}\sqrt{2}\pi\left(r^2\right)^{3/4}\right)}{3\sqrt{3}}+\frac{2\pi\mathrm{ber}_{-\frac{2}{3}}\left(\frac{2}{3}\sqrt{2}\pi\left(r^2\right)^{3/4}\right)}{3\sqrt{3}}$ (9)	$1-\exp\left(-\frac{2}{3(2\pi)^2}k^3\right)$ (10)	3
Hyperbolic secant $g_2(r)$	1	$1-\mathrm{sech}(\pi r)$ (11)	$1-\mathrm{sech}(k/2)$ (12)	2
Hyperbolic secant $g_2(r)$[49]	2	$1-\mathrm{sech}(2\sqrt{\pi G}r)$ (13)	No closed analytical form	2
Hyperbolic secant $g_2(r)$	3	$1-\mathrm{sech}\left(\frac{\pi^{4/3}}{2^{1/3}}r\right)$ (14)	$1-\frac{2^{2/3}\sqrt[3]{\pi}\tanh\left(\frac{k}{2^{2/3}\sqrt[3]{\pi}}\right)\mathrm{sech}\left(\frac{k}{2^{2/3}\sqrt[3]{\pi}}\right)}{k}$ (15)	2
Gaussian-damped polynomial	2	$1-\frac{1}{3}e^{-\pi r^2}\left(4\pi^2r^4-8\pi r^2+3\right)$ (16)	$1-\frac{e^{-\frac{k^2}{4\pi}}\left(k^4-8\pi k^2+12\pi^2\right)}{12\pi^2}$ (17)	2
Hermite–Gaussian[50]	1	$1-\lambda\left(4r^4-12r^2+3\right)e^{-\frac{r^2}{2}}$ (18)	$1-\lambda\sqrt{2\pi}\left(-4k^4+12k^2-3\right)e^{-\frac{k^2}{2}}$ (19)	0
Hyposurficial[51]	3	$1+\frac{\exp\left(-r^*\right)}{4\pi}-\frac{\exp\left(-r^*\right)\sin\left(r^*\right)}{r^*}$ (20)	$\frac{6k^{*8}+12k^{*6}+19k^{*4}+24k^{*2}+16}{6\left(k^{*2}+1\right)^2\left(k^{*2}-2k^*+2\right)\left(k^{*2}+2k^*+2\right)}$ (21)	0
Ghost RSA[52]	1	$\frac{2\Theta(2r-1)}{2-(1-r)\Theta(2-2r)}$ (22)	$1-4\cos\left(k\right)\left[\mathrm{Ci}\left(\frac{3k}{2}\right)+\mathrm{Ci}(2k)\right]-4\sin\left(k\right)\left[\mathrm{Si}\left(\frac{3k}{2}\right)+\mathrm{Si}(2k)\right]-\frac{2\sin\left(k\right)}{k}$ (23)	0
Ghost RSA[53]	2	$\frac{2\Theta\left(r^*-1\right)}{2-\frac{2}{\pi}\left[\cos^{-1}\left(\frac{r^*}{2}\right)-\frac{r^*}{2}\sqrt{1-\frac{r^{*2}}{4}}\right]\Theta\left(2-r^*\right)}$ (24)	No closed analytical form	0
Antihyperuniform[54]	1, 2, 3	$\Theta(r/D-1)\left(\frac{A}{(r/D)^{d-\frac{1}{2}}}+1\right)$ (25)	See Appendix	$-\frac{1}{2}$

we also study a case of prescribed pair statistics whose functional forms are motivated by the polymer reference interaction site model (PRISM)[55,56] and show that they can be realized. It is important to note that one can realize many designed pair functions at different densities and temperatures other than those explicitly shown in Table I, either by creating linear combinations of our pair functions or by applying our inverse procedure to other desirable functional forms. We further show that our pair functions exhibit distinctly different translational order metric τ (defined in Sec. V)[57] and self-diffusion coefficients $\mathcal{D}$, and that τ and $\mathcal{D}$ are inversely related for our 3D models.

Section II provides a comprehensive description of our inverse methodology. In Sec. III, we present our results for the target and optimized pair statistics and the corresponding effective potentials. In Sec. IV, we probe the realizability of the prescribed polymer pair statistics motivated by the PRISM model. In Sec. V, we show that the translational order and the self-diffusion coefficients are inversely correlated to one another for our 3D designs. In Sec. VI, we discuss the implications of our work for outstanding problems in statistical mechanics and materials design via classical and quantum systems in and out of equilibrium.

II. INVERSE METHODOLOGY

To determine effective classical one- and two-body interactions from prescribed pair statistics, we employ an accelerated version of an inverse algorithm that we developed recently,[33] which enables one to recover the unique pair potential corresponding to given pair statistics, as dictated by Henderson's theorem.[58] Our current methodology improves upon the original one[33] by incorporating

31 January 2024 15:02:42

Published under an exclusive license by AIP Publishing

automatic differentiation[59] and canonical ensemble reweighing[60] techniques, achieving significantly faster convergence of potentials. A flowchart of the algorithm is shown in Fig. 1.

The methodology uses a parameterized potential $v(r;\ \mathbf{a})$, whose initial functional form is informed by the small- and large-distance behaviors of the target pair statistics.[35] The scalar components a_j of the potential parameter vector $\mathbf{a}$ are of three types: dimensionless energy scales ε_j, dimensionless distance scales σ_j, and dimensionless phases θ_j;[33] see Appendix B for the potential parameters in each case. To obtain an initial form of the small- and intermediate-r behavior of $v(r;\ \mathbf{a})$, we numerically fit the hypernetted chain (HNC) approximation for the target pair statistics; see details in Ref. 33. The large-r behavior of $v(r;\ \mathbf{a})$ is given by the target direct correlation function $c(r)$ under mild conditions.[4,33] For hyperuniform targets, the large-r asymptotic form of $v(r) \sim -c(r)$ is given by Eq. (28).[35] That is, the potential is long-ranged in the sense that its volume integral is unbounded. Thus, one requires a neutralizing background one-body potential to maintain stability,[1,35,61,62] and the Ewald summation technique[63] is used to compute the total potential energy. For nonhyperuniform targets, the volume integral of $c(r)$ is bounded, and one only requires two-body interactions.

Once the initial form of $v(r;\ \mathbf{a})$ is chosen, the low-storage Broyden–Fletcher–Goldfarb–Shanno (BFGS) algorithm[64] is used to minimize an objective function $\Psi(\mathbf{a})$ based on the distance between target and trial pair statistics in both direct and Fourier spaces,

$$\Psi(\mathbf{a}) = \rho \int_{\mathbb{R}^d} w_{g_2}(\mathbf{r})\left(g_{2,T}(\mathbf{r}) - g_2(\mathbf{r};\mathbf{a})\right)^2 d\mathbf{r} + \frac{1}{\rho(2\pi)^d}\int_{\mathbb{R}^d} w_S(\mathbf{k})\left(S_T(\mathbf{k}) - S(k;\mathbf{a})\right)^2 d\mathbf{k}, \quad (26)$$

where $g_{2,T}(\mathbf{r})$ and $S_T(\mathbf{k})$ are the target pair statistics, $w_{g_2}(\mathbf{r})$ and $w_S(\mathbf{k})$ are the weight functions, and $g_2(\mathbf{r};\ \mathbf{a})$ and $S(\mathbf{k};\ \mathbf{a})$ are the equilibrated pair statistics under $v(r;\ \mathbf{a})$ obtained from Monte Carlo simulations. As done in our previous studies,[24,33,65] we use Gaussian weight functions: $w_{g_2}(r) = \exp\left[-(r/4)^2\right]$ and $w_S(k) = \exp[-(k/2)^2]$.

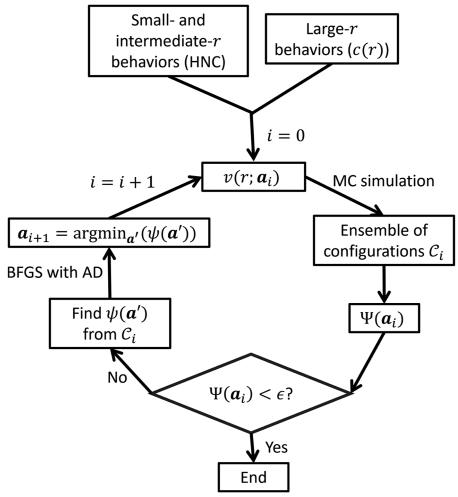


FIG. 1. Flowchart of the inverse methodology developed in this work, assuming a homogeneous target system.

The BFGS algorithm requires the gradient of the objective function $\Psi(\mathbf{a})$. In this work, we replace the finite difference method in Ref. 33 with automatic differentiation (AD), a technique that quickly generates precise gradients on input parameters of computer programs by repeatedly applying the chain rule.[59] AD has the advantage that its computational complexity for gradients is independent of the number of parameters.[59] Because standard implementations of AD[66] can only compute gradients for deterministic functions, but $\Psi(\mathbf{a})$ depends on stochastically simulated pair statistics, one requires a deterministic function $\psi(\mathbf{a})$ that approximates $\Psi(\mathbf{a})$ in the vicinity of the given $\mathbf{a}$. In this work, we define $\psi(\mathbf{a})$ via the canonical ensemble reweighing technique[60] described below.

Let $\mathcal{C}_i$ be a set of configurations equilibrated under $v(r;\ \mathbf{a}_i)$ drawn from a simulated canonical ensemble in iteration i, and let $\mathbf{a}'$ be a perturbed potential parameter in the vicinity of $\mathbf{a}_i$. The ensemble-averaged pair statistics under $v(r;\ \mathbf{a}')$ are estimated by reweighing the pair statistics of each configuration in $\mathcal{C}_i$ by a Boltzmann factor involving the difference in total configurational energies $\Phi(\mathbf{r}^N) = \sum_{i<j}^N v(|\mathbf{r}_i - \mathbf{r}_j|)$ under $v(r;\ \mathbf{a}_i)$ and $v(r;\ \mathbf{a}')$,[60] i.e.,

$$\varphi(x;\mathbf{a}') = \frac{\sum_{\mathbf{r}^N\in\mathcal{C}_i}\varphi(x;\mathbf{r}^N)\exp\left[-(\Phi(\mathbf{r}^N;\mathbf{a}') - \Phi(\mathbf{r}^N;\mathbf{a}_i))/T\right]}{\sum_{\mathbf{r}^N\in\mathcal{C}_i}\exp\left[-(\Phi(\mathbf{r}^N;\mathbf{a}') - \Phi(\mathbf{r}^N;\mathbf{a}_i))/T\right]}, \quad (27)$$

where $\varphi(x;\ \mathbf{r}^N)$ is $g_2(r)$ or $S(k)$ computed from each configuration $\mathbf{r}^N$ in $\mathcal{C}_i$. The approximate objective function $\psi(\mathbf{a}')$ at the perturbed parameters $\mathbf{a}'$ can then be computed by inserting (27) into (26). For a fixed set of simulated configurations $\mathcal{C}_i$, $\psi(\mathbf{a}')$ is a deterministic function of $\mathbf{a}'$. Thus, one can apply BFGS optimization with AD-generated gradients to find the optimal parameters $\mathbf{a}_{i+1}$ that minimize $\psi(\mathbf{a}')$. In the next iteration, simulations are performed under $v(r;\ \mathbf{a}_{i+1})$ to obtain a new set of configurations $\mathcal{C}_{i+1}$. The iterations repeat until $\Psi(\mathbf{a}_i)$ computed from $\mathcal{C}_i$ is smaller than some given convergence threshold ϵ, set to be 10^{-3} in this study. If convergence is not achieved, a different set of basis functions is chosen, and the optimization process is repeated. Note that this inverse methodology accelerates our original algorithm[33] as it requires just one simulation per iteration for n potential parameters, as opposed to $2n$ simulations using finite differences. For systems away from the critical point, convergence can be achieved within 5 h on an Intel 2.8 GHz CPU with 15 cores and 4 GB of memory per core.

For systems near the critical point, common inverse methods based on predictor–corrector approaches, such as iterative Boltzmann inversion (IBI),[67] do not perform well due to critical slowing down and the large number of iterations required for the trial potential to converge.[33] IBI updates a binned trial potential $v(r)$ based on the difference between the target and simulated $g_2(r)$ in each iteration. By contrast, our inverse method uses an analytical potential form dictated by statistical–mechanical theory. This form is robust to variations in the large-r behavior of the simulated $g_2(r)$, which can cause undesirable long-range oscillation in $v(r)$ in the IBI approach. Thus, the potential in our method converges in much fewer iterations. For the 1D antihyperuniform state, which is the most challenging target among the ones studied here, convergence was achieved within 24 h.

31 January 2024 15:02:42

Published under an exclusive license by AIP Publishing

III. RESULTS FOR DESIGNED PAIR CORRELATION FUNCTIONS

In this section, we describe the targeted analytical forms for pair statistics in direct and Fourier spaces in various space dimensions summarized in Table I and then show their realizability by equilibrium states with up to pair interactions via the inverse algorithm described in Sec. II. For each target, we show that the optimized pair statistics precisely match the prescribed functions. The initial functional forms of the effective potentials are chosen based on the small- and large-r behaviors of the target pair statistics, as dictated by statistical mechanical theory.[33] The asymptotic decay rate of the direct correlation function $c(r)$, which is linked to the total correlation function $h(r) = g_2(r) - 1$ via the Ornstein–Zernike equation,[68] determines whether one needs both one-body and two-body interactions (for hyperuniform states) or only two-body interactions (for nonhyperuniform states); see Sec. II for details. Note that certain pair interactions for hyperuniform states are not square integrable, but the total energy is nevertheless bounded due to the background one-body interaction that maintains overall charge neutrality.[33,35] Unless otherwise stated, we take $\rho = 1$, and the lengths are expressed in units of $\rho^{-1/d}$. We also set the reduced temperature k_BT to be unity for all the equilibrium states, where k_B is the Boltzmann constant.

A. D-dimensional hyperuniform Gaussian pair statistics

We consider d-dimensional generalizations of Gaussian pair statistics given by Eqs. (3) and (4) in Table I. These targets are hyperuniform, with $\alpha = 2$ in Eq. (1). Note that the pair functions are self-similar under Fourier transformations up to scaling and are independent of the dimensionality. Gaussian pair statistics incorporate soft-core short-ranged repulsions found in macromolecules and, thus, are commonly used to model polymer systems.[56,69–71] The Gaussian pair functions represent the low-density, high-temperature limit of the pair statistics for the popular Gaussian-core model,[12,72–74] which is known to exhibit anomalous phase behaviors, such as reentrant melting.[74,75]

Figures 2(a) and 2(b) show the target and optimized $g_2(r)$ and $S(k)$, respectively, for the hyperuniform Gaussian pair statistics in one, two, and three dimensions. It is clear that the target and optimized pair statistics agree very well with one another. The precise form of the corresponding effective potential is given in the Appendix and plotted in Fig. 12(a). Torquato[35] showed that for hyperuniform targets, the long-ranged asymptotic form of $v(r)$ is given by

$$v(r) \sim \begin{cases} r^{-(d-\alpha)}, & d \neq \alpha, \\ -\ln(r), & d = \alpha, \end{cases} \tag{28}$$

which can be regarded as a generalized Coulombic interaction of "like-charged" particles. For $\alpha = 2$, the long-ranged parts of the potentials are given by the Coulomb interactions $v(r) \sim r^{-(d-2)}$ in the respective dimensions. Note that for the 2D Gaussian pair statistics, it is known that the effective pair potential is exactly given by the 2D Coulombic interaction $v(r) = -2\ln(r)$.[20] Our inverse procedure has accurately recovered this potential.

Figures 2(c) and 2(d) show representative configurations of the 2D and 3D equilibrium states with Gaussian pair statistics. Note that

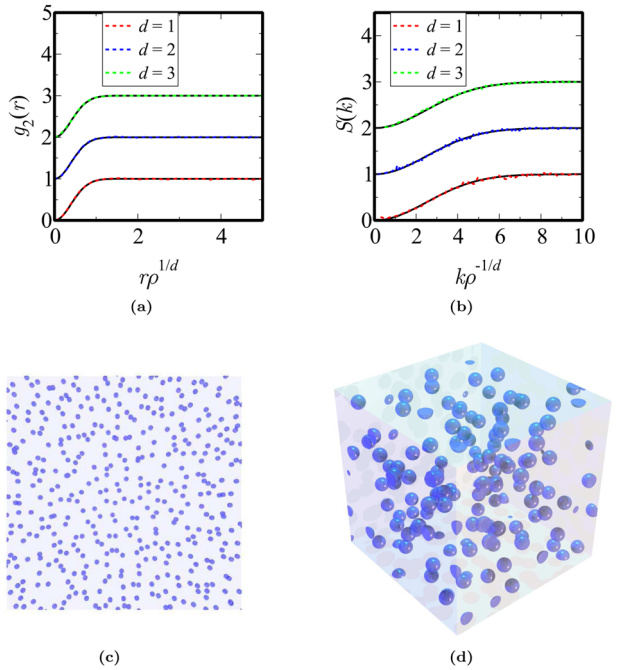


FIG. 2. (a) and (b) Target (solid curves) and optimized (dashed curves) $g_2(r)$ and $S(k)$ for Gaussian pair statistics. For clarity, the pair statistics for $d = 2$ and $d = 3$ are shifted up by 1 and 2, respectively. (c) A 400-particle configuration of the 2D equilibrium state with Gaussian pair statistics. (d) A 125-particle configuration of the 3D equilibrium state with Gaussian pair statistics. The point particles are shown as spheres for visualization purposes.

while particles can get arbitrarily close, both configurations do not contain large clusters or large spherical holes that are void of particles. Indeed, the particles tend to form short chains that are well separated. These observations are consistent with the soft repulsive interactions in the effective potentials.

B. D-dimensional hyperuniform generalized OCP and their Fourier duals

We consider 3D generalizations[32] of the hyperuniform OCP given by Eqs. (5) and (6) as well as the 1D and 3D Fourier duals of OCP given by Eqs. (7)–(10) in Table I. An OCP is an equilibrium system of identical point particles of charge e interacting via the Coulomb potential and immersed in a rigid uniform background of opposite charge to ensure overall charge neutrality.[20] OCPs are classical analogs of the quantum jellium model and are used as a first approximation to dense plasmas.[76] The pair statistics for the 2D OCP, which is equivalent to the Ginibre ensemble, are exactly given by the Gaussian functions (3) and (4).[20]

Zhang and Torquato[32] proposed a generalization of the OCP pair correlation function to arbitrary dimensions, given by

$$g_2(r) = 1 - \exp[-v_1(r)], \tag{29}$$

where $v_1(r)$ is the volume of a d-dimensional sphere of radius r. The corresponding structure factors at $\rho = 1$ are hyperuniform with

31 January 2024 15:02:42

Published under an exclusive license by AIP Publishing

$\alpha = 2$. For $d = 1$, the generalized OCP pair statistics are identical to a Lorenztian target,

$$g_2(r) = 1 - \exp(-2r), \tag{30}$$

which has been shown to be realizable by a determinantal point process.[19] Thus, we study the 3D case here, whose realizability is unknown.

For the d-dimensional Fourier duals of OCP, the structure factors assume the same form as the OCP pair correlation function (29) up to scaling, i.e.,

$$S(k) = 1 - \exp[-v_1(k/2\pi)], \tag{31}$$

for which the exponent in Eq. (1) is given by $\alpha = d$. This implies that $S(k)$ is nonanalytic at the origin for any odd dimension and, thus, the corresponding $g_2(r)$ has power-law asymptotic r^{-2d}.[33]

We achieved excellent agreement between target and optimized pair statistics for both OCP and its Fourier dual. Figures 3(a) and 3(b) show the target and optimized pair statistics for the 3D OCP. The corresponding configuration [Fig. 3(c)] is similar to that for the 3D Gaussian pair statistics, as both systems have soft-core repulsive interactions. However, the OCP has larger force magnitudes as $r \to 0$, as shown in Fig. S1 in the supplementary material, which plots the forces $-dv(r)/dr$ corresponding to the effective potentials for our 3D hyperuniform models. The difference in the small-r repulsion is due to the fact that the OCP $g_2(r)$ increases as r^d in the vicinity of the origin, rather than r^2 for the Gaussian. Our capacity to design systems with varying magnitudes of short-range repulsive forces enables coarse-grained modeling of polymers with different levels of chain rigidity and penetrability.[77,78]

Figures 3(d)–3(f) present the results for the Fourier dual of OCP in the first three spatial dimensions. Note that the exponent α in (1) for the simulated 3D Fourier dual of OCP, i.e., $\alpha = 3$, is larger than that of any other positive-temperature equilibrium states known previously. The largest known exponent prior to this work was $\alpha = 2$ for systems under Coulombic interactions.[35] Our result here shows that states with $\alpha > 2$ can be attained by pair potentials that are longer-ranged than the d-dimensional Coulombic interactions. While it is experimentally challenging to create nanoparticles with such long-range molecular interactions, they are hypothesized to be attainable by topological defects in the gauge fields in the form of space-time instantons.[79,80] Hyperuniform systems with large α are desirable for optical purposes because they tend to be effectively transparent for a wide range of wave numbers compared to non-hyperuniform ones.[81] We note further that despite having strong

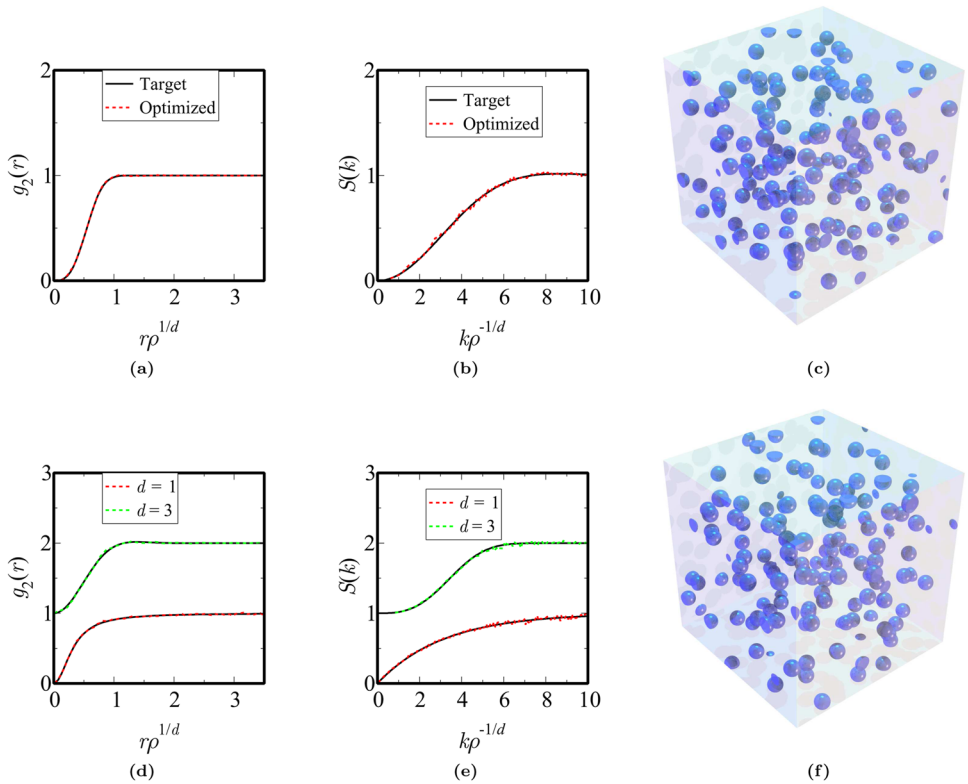


FIG. 3. (a) and (b) Target and optimized $g_2(r)$ and $S(k)$ for 3D generalized OCP. (c) A 125-particle configuration of the 3D equilibrium state with the generalized OCP pair statistics. (d) and (e) Target (solid curves) and optimized (dashed curves) for 1D and 3D Fourier duals of OCP. For clarity, the pair statistics for the 3D case are shifted up by 1. (f) A 125-particle configuration of the 3D equilibrium state with the Fourier dual OCP pair statistics. In all 3D configurations, the point particles are shown as spheres for visualization purposes.

31 January 2024 15:02:42

Published under an exclusive license by AIP Publishing

large-r repulsion, particles in the 3D Fourier dual of OCP are less repulsive at small r than those in the 3D OCP, as shown in Fig. S1.

C. d-dimensional hyperuniform hyperbolic secant function $g_2(r)$

We consider the hyperuniform states characterized by the hyperbolic secant function $g_2(r)$ given by Eqs. (11)–(15) in Table I. As in the case of the Gaussian pair statistics, these are soft-core models, and the structure factors scale as k^2 at small k. Moreover, in the 1D case, $g_2(r)$ and $S(k)$ are self-similar up to scaling. We have chosen this target for its capability to model polymers with softer repulsive interactions than the Gaussian core[82] and to generate configurations with a higher degree of clustering than the Gaussian pair statistics. A hyperbolic secant probability distribution is *leptokurtic*, i.e., it has a smaller probability density around the mean but a heavier tail than the corresponding Gaussian distribution with the same mean and variance.[82] For a hyperuniform state at unit number density, the hyperbolic secant $g_2(r)$ rises more rapidly at small r but decays to unity more slowly at large r compared to the Gaussian $g_2(r)$. Thus, we propose that hyperbolic secant pair functions and other leptokurtic functions[82] can be applied to describe polymer systems with "ultrasoft" particles, such as star polymers.[83,84]

Figures 4(a) and 4(b) show the target and optimized pair statistics for the hyperbolic secant $g_2(r)$. Because these pair functions imply softer core interactions than those for the Gaussian pair statistics, the corresponding 3D configuration [Fig. 4(c)] contains more clusters with four or more closely spaced particles with pair distances $r \le 0.4\rho^{-1/3}$ compared to the Gaussian case. Clusters in the latter system are primarily dimer and trimer; see Fig. 2(d). Cluster statistics can be quantified by mapping the point configurations to a two-phase medium generated by decorating each point particle with a sphere of a certain radius and then using theoretical tools from percolation theory.[7,85,86] Figure S1 shows that the effective potential for the hyperbolic secant $g_2(r)$ is the least repulsive at small r among the 3D hyperuniform models. As remarked in Sec. III B, softer interactions are useful in describing polymer molecules with high penetrability.

D. 2D hyperuniform Gaussian-damped polynomial and 1D nonhyperuniform Hermite–Gaussian pair statistics

We consider the 2D hyperuniform Gaussian-damped polynomial pair statistics given by Eqs. (16) and (17) in Table I, as well as the 1D nonhyperuniform Hermite–Gaussian pair statistics given by (18) and (19). These pair functions mimic those found in dense polymer systems, which often exhibit oscillations due to the coordination shells.[87,88] In both cases, the pair functions are self-similar under Fourier transformations up to scaling. Notably, the forms of the 2D pair functions are chosen to closely resemble the pair statistics of polymer chains modeled by freely rotating fused hard spheres.[88] The oscillatory $g_2(r)$ function [Fig. 5(a)] dictates that the corresponding many-particle system must have significant particle clustering. In addition, note that the form of the 1D total correlation function $h(r)$ is a Hermite–Gaussian function of order 4. Hermite–Gaussian functions have been used to describe semiflexible polymers such as DNA and actin.[89] We can precisely realize how the pair functions in both cases, as shown in Figs. 5 and 6. The effective potentials for both cases are oscillatory and may be realized by "sticky" macromolecules, such as DNA-coated nanoparticles, as one can achieve precise control of attraction and repulsion at specific radial distances for these particles;[90,91] see Appendix for the precise functional forms. Compared to the configuration for the 2D Gaussian pair function [Fig. 2(c)], the configuration for the 2D Gaussian-damped polynomial [Fig. 5(c)] contains considerably fewer chains. Instead, it contains many clusters with more than four closely spaced particles due to the peak in $g_2(r)$ at $r\rho^{1/2} \sim 0.6$. Despite this heterogeneity on the small to intermediate scale, Fig. 5(c) is homogeneous on the large scale as a result of the prescribed hyperuniformity, i.e., there are no large clusters or spherical holes void of particles on the order of the system size.

E. 3D hyposurficial state

We consider, for the first time, the possible realizability of the nonhyperuniform hyposurficial state specified by Eqs. (20) and (21) in Table I, which apply in three dimensions. Hyposurficial systems

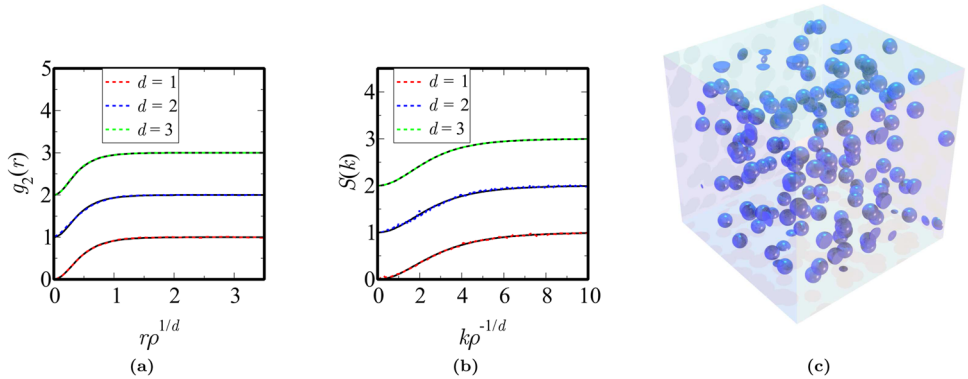


FIG. 4. (a) and (b) Target (solid curves) and optimized (dashed curves) for 1D–3D hyperbolic secant $g_2(r)$. For clarity, the pair statistics for $d = 2$ and $d = 3$ are shifted up by 1 and 2, respectively. (c) A 125-particle configuration of the 3D equilibrium state with hyperbolic secant $g_2(r)$. The point particles are shown as spheres for visualization purposes.

31 January 2024 15:02:42

Published under an exclusive license by AIP Publishing

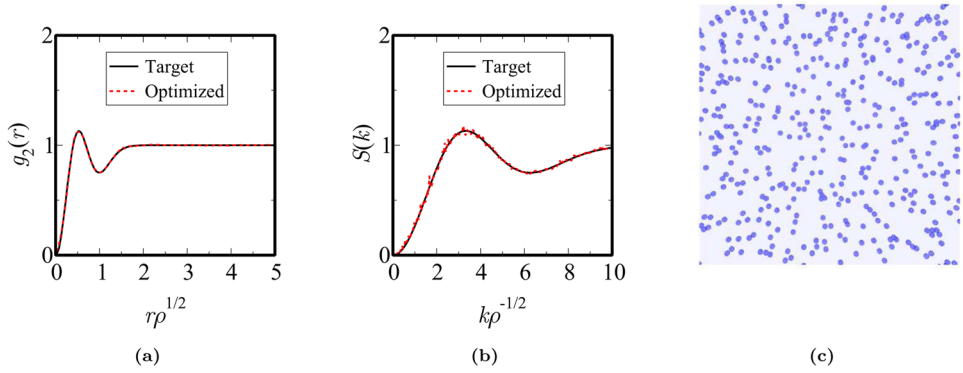


FIG. 5. (a) and (b) Target and optimized $g_2(r)$ and $S(k)$ for the 2D Gaussian-damped polynomial pair statistics. (c) A 400-particle configuration of the 2D equilibrium state with the Gaussian-damped polynomial pair statistics.

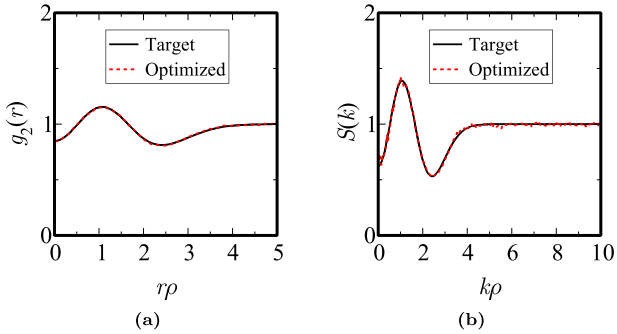


FIG. 6. Target and optimized (a) $g_2(r)$ and (b) $S(k)$ for the 1D hyposurficial Hermite–Gaussian $g_2(r)$ with $\lambda = 1/20$.

are a special class of nonhyperuniform states that can be observed in nonequilibrium phase transitions in amorphous ices,[92] supercritical equilibrium liquids,[33] and certain hard-core systems.[34] They behave like ideal gases in their large-scale local number variance $N(R)$ because they lack a "surface-area" term proportional to R^{d-1} in the growth of $N(R)$, i.e., $\sigma^2(R) \sim AR^d + o(R^{d-1})$ as $R \to \infty$, where A is a positive constant. Hyposurficial pair statistics obey the following sum rule:[34]

$$\int_0^\infty r^d h(r) dr = 0, \tag{32}$$

which implies that they must generally contain both negative and positive correlations. Ideal gases are trivially hyposurficial. Figure 7 shows that we can precisely realize the designed hyposurficial target. The configuration [Fig. 7(c)] shows spatial heterogeneities, i.e., there exists significant particle clustering as well as large spherical holes void of particles.

F. 1D and 2D ghost RSA

We consider the nonhyperuniform pair statistics corresponding to the 1D and 2D ghost RSA packings, given by Eqs. (22)–(24) in Table I. The nonequilibrium ghost RSA process[23,27] is a special case of a generalization of the standard RSA process[7,93,94] and is the only known model for which all n-particle correlation functions are

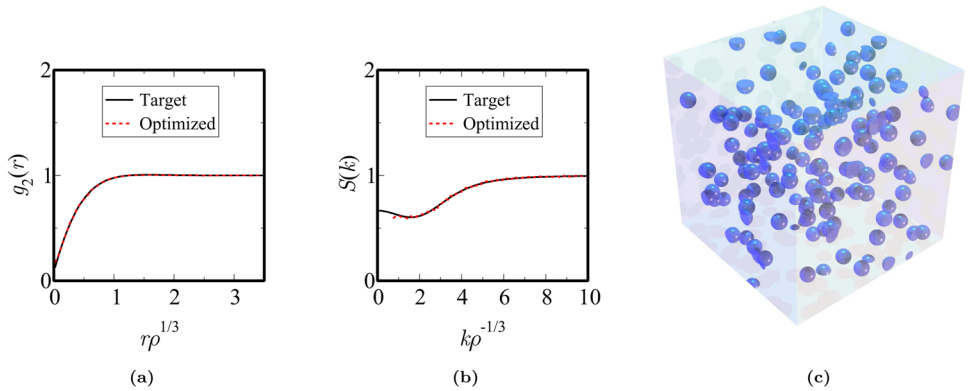


FIG. 7. (a) and (b) Target and optimized $g_2(r)$ and $S(k)$ for the 3D hyposurficial state. (c) A 125-particle configuration of the 3D equilibrium hyposurficial state. The point particles are shown as spheres for visualization purposes.

31 January 2024 15:02:42

Published under an exclusive license by AIP Publishing

exactly solvable.[23] In the ghost RSA process, spherical "test" particles of diameter D are added continually to $\mathbb{R}^d$ during time $t \geq 0$ according to a translationally invariant Poisson process of density η per unit time, i.e., η is the number of points per unit volume and time, here taken to be unity without loss of generalization. A test sphere centered at position $\mathbf{r}$ at time t is retained if and only if it does not overlap with any test sphere added in the time interval $(0, t)$.[23] The saturation packing fraction for the ghost RSA process is $\phi(t = +\infty) = 1/2^d$.[23]

We have previously shown that the 3D ghost RSA pair statistics at the terminal packing fraction are realizable by an equilibrium state with up to pair interactions.[24] Here, we investigate whether the same is true for $d = 1$ and 2. It is not obvious that the ghost RSA processes are realizable in these lower dimensions because, generally speaking, it is known that the lower the space dimension, the more difficult it is to satisfy realizability conditions.[27] This dimensionality effect arises on account of the decorrelation principle,[27] which states that spatial correlations that exist for a particular model in lower dimensions diminish as the space dimension becomes larger.

Figure 8 shows that we can achieve the nonequilibrium 1D and 2D ghost RSA packings with the effective potentials in Fig. 12(i), which contain both a hard-core and soft repulsion beyond the diameter. Effective soft repulsion ensures that particles are well-separated and corresponds to the exclusion of real particles by the "ghost" test particles in the nonequilibrium process. This combination of hard core and soft repulsion in $v(r)$ can be found in colloidal suspensions of highly charged nanoparticles.[95] Note that the soft repulsion is more significant for the 1D case than the 2D case, reflecting the aforementioned decorrelation principle.[27] For $d = 3$, the ghost RSA $g_2(r)$[23] is nearly equal to unity for $D \leq r \leq 2D$, and the soft repulsion in its effective potential[24] is weaker than that in the 2D case. In the limit that $d \to \infty$, the ghost RSA $g_2(r)$ approaches the unit-step $g_2(r)$,[27] and the effective potential would consequently converge to that of the hard-sphere potential. The effective potentials also exhibit weak attractive wells [Fig. 8(a)], which offset the oscillations in $g_2(r)$ that would occur in a pure equilibrium hard-sphere system, ensuring that $g_2(r)$ is flat beyond two diameters.

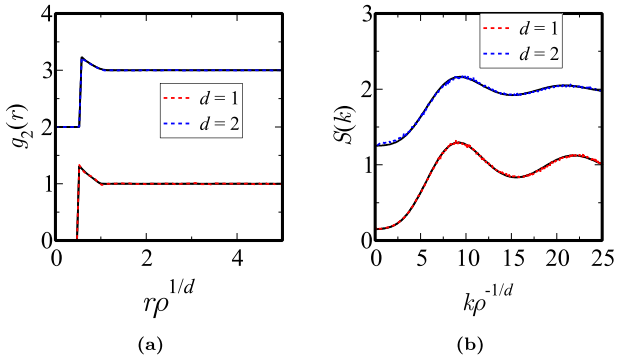


FIG. 8. Target (solid curves) and optimized (dashed curves): (a) $g_2(r)$ and (b) $S(k)$ for the 1D and 2D ghost RSA packings. For clarity, the $g_2(r)$ curve for $d = 2$ is shifted up by 2 and the $S(k)$ curve for $d = 2$ is shifted up by 1.

G. d-Dimensional antihyperuniform pair statistics

We study the antihyperuniform pair statistics (25) in one-, two-, and three-dimensions. Note that the target $g_2(r)$ functions imply a hard core with diameter D. The functional forms of $S(k)$ as well as the packing fraction $\phi = \rho v_1(D/2)$ and the parameter A are given in Appendix A. The values of ϕ and A chosen ensure the necessary condition that $S(k)$ must be nonnegative at all k. As mentioned in the Introduction, $S(k)$ for an antihyperuniform state has the small-k scaling behavior $S(k) \sim k^{\alpha}$, where α is negative. This divergence behavior of $S(k)$ at small k is characteristic of fluids at thermal critical points, which can have fractal-like structures.[38,40] For our antihyperuniform targets in any dimension, we take $\alpha = -1/2$, implying that $h(r)$ has a long-ranged power-law decay behavior at large r as $h(r) \sim r^{-(d-1/2)}$.[35] Realizable systems with such pair statistics would correspond to a different universality class than the Ising class, which gives the large-r behavior $h(r) \sim r^{-(d-2+\eta)}$, where $\eta = 1/4$ for $d = 2$ and $\eta = 0.036$.[42]

Computing equilibrium properties at critical points using Monte Carlo or molecular dynamics simulations is known to be challenging due to the critical slowing down phenomena, i.e., the relaxation time to the equilibrium state diverges at the critical point.[38,96] Our inverse method reduces the time required to reach the targeted critical-point pair statistics compared to previous methods, as it uses parameterized analytical pair potentials rather than binned potentials;[33] see Sec. II for details. We have realized the

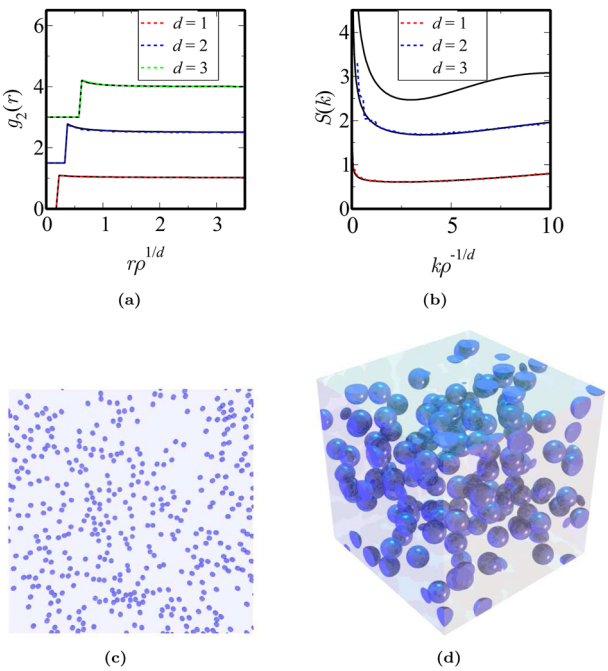


FIG. 9. (a) and (b) Target (solid curves) and optimized (dashed curves) $g_2(r)$ and $S(k)$ for d-dimensional antihyperuniform pair statistics (25). For clarity, $g_2(r)$ for $d = 2$ and $d = 3$ are shifted up by 1.5 and 3, respectively, and $S(k)$ for $d = 2$ and $d = 3$ are shifted up by 1 and 2, respectively. (c) A 400-particle configuration of the 3D equilibrium antihyperuniform state. (d) A 125-particle configuration of the 3D equilibrium antihyperuniform state. The disk and sphere diameters in the configurations are the hard-core diameter D.

31 January 2024 15:02:42

Published under an exclusive license by AIP Publishing

antihyperuniform critical-point pair statistics in one, two, and three dimensions, as shown in Fig. 9. The 2D and 3D critical-point states [Figs. 9(c) and 9(d)] clearly show large clusters and large empty spherical holes on the order of the system size, confirming that antihyperuniformity corresponds to divergent long-range number density fluctuations.

The realizability of the 1D critical state is unusual because it is commonly thought that phase transitions cannot exist in 1D systems, but this is only true when the interactions are sufficiently short-ranged.[97,98] Indeed, in the Appendix, we show that the effective pair potential has a long-ranged attractive part, i.e., $v(r) \sim -r^{-(d-1/2)}$ as $r \to \infty$. This long-range behavior in the interaction explains why our 1D, 2D, and 3D critical-point states do not belong to the Ising universality class that is characterized by short-ranged interactions.[39–42]

IV. REALIZABILITY OF PAIR STATISTICS FROM A 3D POLYMER MODEL

To illustrate that our procedure can be used to guide experimental polymer design, we now examine a case of prescribed pair statistics whose functional forms are motivated by the PRISM model.[55,56] According to this model, the total correlation function for polymer chains is given by[56]

$$h(r;\rho) = \frac{3}{4}\sqrt{\frac{3}{\pi}}e^{-\frac{1}{4}(3r^2)}\tilde{\xi}'_\rho\left(1-\frac{1}{2\tilde{\xi}_\rho^2}\right) - \frac{\tilde{\xi}'_\rho\left(1-\frac{1}{2\tilde{\xi}_\rho^2}\right)^2 e^{\frac{1}{3\tilde{\xi}_\rho^2}}\left[e^{\frac{r}{\tilde{\xi}_\rho}}\operatorname{erfc}\left(\frac{1}{\sqrt{3}\tilde{\xi}_\rho}+\frac{\sqrt{3}r}{2}\right) - e^{-\frac{r}{\tilde{\xi}_\rho}}\operatorname{erfc}\left(\frac{1}{\sqrt{3}\tilde{\xi}_\rho}-\frac{\sqrt{3}r}{2}\right)\right]}{2r}, \tag{33}$$

where lengths are measured in units of the radius of gyration R_G, $\tilde{\xi}_\rho = 1/[\sqrt{2}(\pi\sqrt{2}\rho+1)]$, and $\tilde{\xi}'_\rho = 1/(2\pi\rho)$. The corresponding $S(k)$ is also known analytically.[56] Yatsenko *et al.*[56] showed that for $0.86 < \rho < 1.62$, Eq. (33) accurately describes the experimental radial distributions of polyethylene and polypropylene melts at small to intermediate r. However, the experimental realizability of (33) outside of this density range has not been tested. We have applied our inverse algorithm to Eq. (33) at $\rho = 0.5$ and have achieved excellent agreement between the target and optimized pair functions by a soft-core effective potential, as shown in Fig. 10. These hypothetical pair statistics might be experimentally achievable by polymer melts at low density, e.g., via polyethylene molecules with a smaller number of monomers per chain than those considered in Ref. 56.

V. TRANSLATIONAL ORDER METRICS AND SELF-DIFFUSION COEFFICIENT

To demonstrate that our designed analytical pair functions enable one to achieve a wide range of structural order and physical properties, we compute the translational order metric τ[57] and the self-diffusion coefficient $\mathcal{D}$[12] for the 3D states studied here. The τ order metric is defined by[57]

$$\tau = \rho\int h^2(r)d\mathbf{r} = \frac{\rho}{(2\pi)^d}\int_{\mathbb{R}^d}\tilde{h}^2(k)d\mathbf{k}, \tag{34}$$

where $\tilde{h}(k)$ is the Fourier transform of $h(r)$. This order metric measures deviations of pair statistics from those of the uncorrelated (Poisson) distribution $g_2(r) = 1$. Since both positive and negative correlations contribute to the integral, due to the fact that $h(r)$ is squared, τ measures the degree of translational order across all length scales. It vanishes for the Poisson distribution and diverges for an infinite crystal,[99] and it is a positive bounded number for correlated disordered systems without long-range order (i.e., Bragg peaks).[100]

To compute the self-diffusion coefficients, we utilize the semi-empirical scaling laws developed by Rosenfeld.[101] The reduced self-diffusion coefficient $\mathcal{D}\rho^{1/3}T^{1/2}$ for 3D fluids in the dilute limit is given by[101]

$$\mathcal{D}\rho^{1/3}T^{1/2} = 0.37(-s_2)^{-2/3}, \tag{35}$$

where

$$s_2 = -(\rho/2)\int_{\mathbb{R}^d}\{g_2(r)\ln[g_2(r)] - g_2(r) + 1\}d\mathbf{r} \tag{36}$$

is the two-body excess entropy. Equation (35) provides a good approximation for soft-core models with $-s_2 \le 0.5$,[12] which is satisfied by all the soft-core pair statistics in this study. For the ghost RSA and the antihyperuniform packings, which have hard-core interactions, we use the corresponding scaling law,[101]

$$\mathcal{D}\rho^{1/3}T^{1/2} = 0.58\exp(0.78s_2). \tag{37}$$

Figure 11 plots τ against the reduced self-diffusion coefficient, where hyperuniform states are indicated with filled circles.

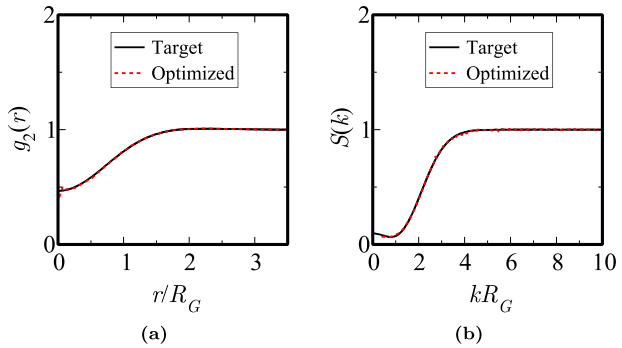


FIG. 10. Target and optimized (a) $g_2(r)$ and (b) $S(k)$ for a hypothetical 3D polymer motivated by the PRISM model with the total correlation function (33) at $\rho = 0.5$.

31 January 2024 15:02:42

Published under an exclusive license by AIP Publishing

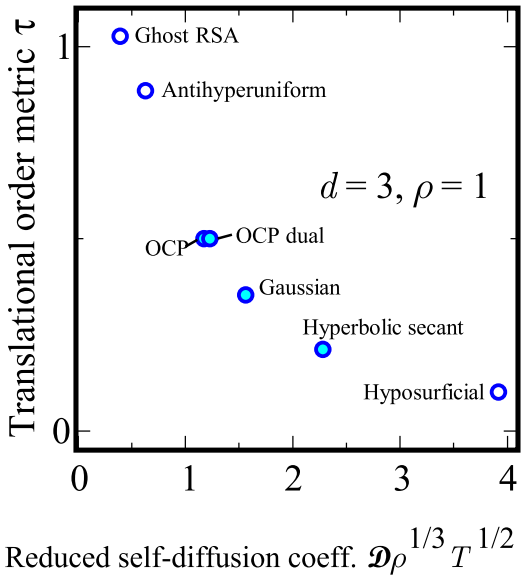


FIG. 11. Translational order metric τ and the reduced self-diffusion coefficient $\mathcal{D}\rho^{1/3}T^{1/2}$ for the 3D pair statistics studied in this work and Ref. 24. The filled circles refer to hyperuniform states, and the unfilled ones refer to nonhyperuniform states.

It is evident that τ and $\mathcal{D}$ are inversely correlated to one another. Pair functions with smaller translational order metrics are closer to the Poisson pair statistics. Thus, in equilibrium states with smaller τ, particles encounter less hindrance from neighboring particles, resulting in higher self-diffusivity. Importantly, τ has a strong positive correlation to $-s_2$,[102] and in the limit that $g_2(r)$ is an infinitesimal perturbation from unity (i.e., from an ideal gas), one has exactly $\tau \sim -4s_2$.[102] Consequently, τ is inversely related to $\mathcal{D}$ via Eq. (35).

The ghost RSA and the antihyperuniform packings have hard-core interactions and achieve higher τ and lower $\mathcal{D}$ because the hard particles are more locally confined due to the frequent collisions with their neighbors.[103] The soft-core hyperuniform states have intermediate τ and $\mathcal{D}$. Figure S1 shows the forces corresponding to the effective potentials for these states, from which it is clear that models with larger magnitudes of small-r repulsion give larger τ and smaller $\mathcal{D}$. The OCP, which has the strongest small-r repulsion among the 3D hyperuniform states, is least diffusive. This is followed by the Fourier dual of OCP, the Gaussian pair statistics, and the hyperbolic secant $g_2(r)$. Interestingly, while OCP and its Fourier dual both have $\tau = 1/2$, the former has a slightly lower self-diffusivity because its $g_2(r)$ scales as r^3 at small r, representing a stronger small-r repulsion than the r^2 scaling for the Fourier dual of OCP. Our observation that particles with soft repulsive interactions are more diffusive than hard-core particles is consistent with the findings for macromolecules via molecular dynamics simulations[78] and for lattice gases via Monte Carlo simulations.[104]

Finally, the hyposurficial state, which lacks both hard-core interactions and hyperuniformity, has the smallest τ and largest $\mathcal{D}$, as its pair statistics are closest to those of an ideal gas. Its low translational order is consistent with the observation in Ref. 105 that hyposurficiality appears to be associated with spatial heterogeneities.

VI. DISCUSSION

We have designed a diverse set of pair functions with varying degrees of disorder across length scales that are realizable by disordered many-particle systems, of which many have novel structural and physical properties. We achieved this via an efficient algorithm that determines equilibrium states with up to pair interactions at positive temperatures. The realizability of the prescribed pair statistics via classical equilibrium states with up to pair interactions is rather strong because once realizability by classical equilibrium systems is shown, it does not exclude the possibility of realizing the same pair statistics via quantum-mechanical equilibrium systems or even nonequilibrium systems.

We have chosen our pair functions based on their capability to generate a wide spectrum of hyperuniform and nonhyperuniform systems with various short-range correlations, including hyperuniform soft-core systems with different small-r repulsive forces, a nonhyperuniform 3D hyposurficial state, 1D and 2D ghost RSA packings, and antihyperuniform packings. These forms of pair functions dictate that the corresponding systems have different cluster sizes from one another. Notably, the 3D Fourier dual of OCP possesses a larger hyperuniformity exponent α than any other positive-temperature equilibrium state known previously, which can be useful in optical applications.[81] We have designed a diverse family of pair functions that are self-similar under Fourier transformations, which means that their low-density and high-density ground-state structures under the effective potentials can be mapped to one another via duality relations.[45,46] Furthermore, we have realized a case of pair statistics whose functional forms are motivated by the PRISM model,[56] indicating that it may be experimentally achieved. Our designed pair functions exhibit distinctly different translational order metric τ and self-diffusion coefficients $\mathcal{D}$. We have shown that for our 3D models, τ and $\mathcal{D}$ are inversely correlated, the same trend of which should be true for the corresponding one- and two-dimensional designs as well. This relationship enables one to easily achieve the desired diffusivity through designed pair functions.

The pair potentials for many states can be experimentally achieved by polymer or nanoparticle systems with tunable chemical components. For example, Yatsenko *et al.*[56] showed that in the limit of long polymer chains, the total distribution function of polyethylene melts with a radius of gyration R_G can be approximated by a Gaussian-damped polynomial,

$$h(\tilde{r},\xi) = -\frac{39}{16}\sqrt{\frac{3}{\pi}}\xi(1+\sqrt{2}\xi)\left(1-\frac{9\tilde{r}^2}{26}\right)\exp\left(-\frac{3\tilde{r}^2}{4}\right), \quad (38)$$

where $\tilde{r} = r/R_G$ and ξ is a parameter inversely proportional to the number density of polymer chains. At small to intermediate $\tilde{r}$, Eq. (38) resembles our Gaussian pair statistics. Interestingly, it has been suggested that hyperuniform pair statistics with soft-core interactions can be achieved by star or bottlebrush polymers.[106] Note that the effective potentials of many of our hyperuniform models[107] contain a Gaussian-damped logarithmic term for their short-ranged parts; see the Appendix for the precise functional forms. Such logarithm-Gaussian pair potential is commonly used

31 January 2024 15:02:42

Published under an exclusive license by AIP Publishing

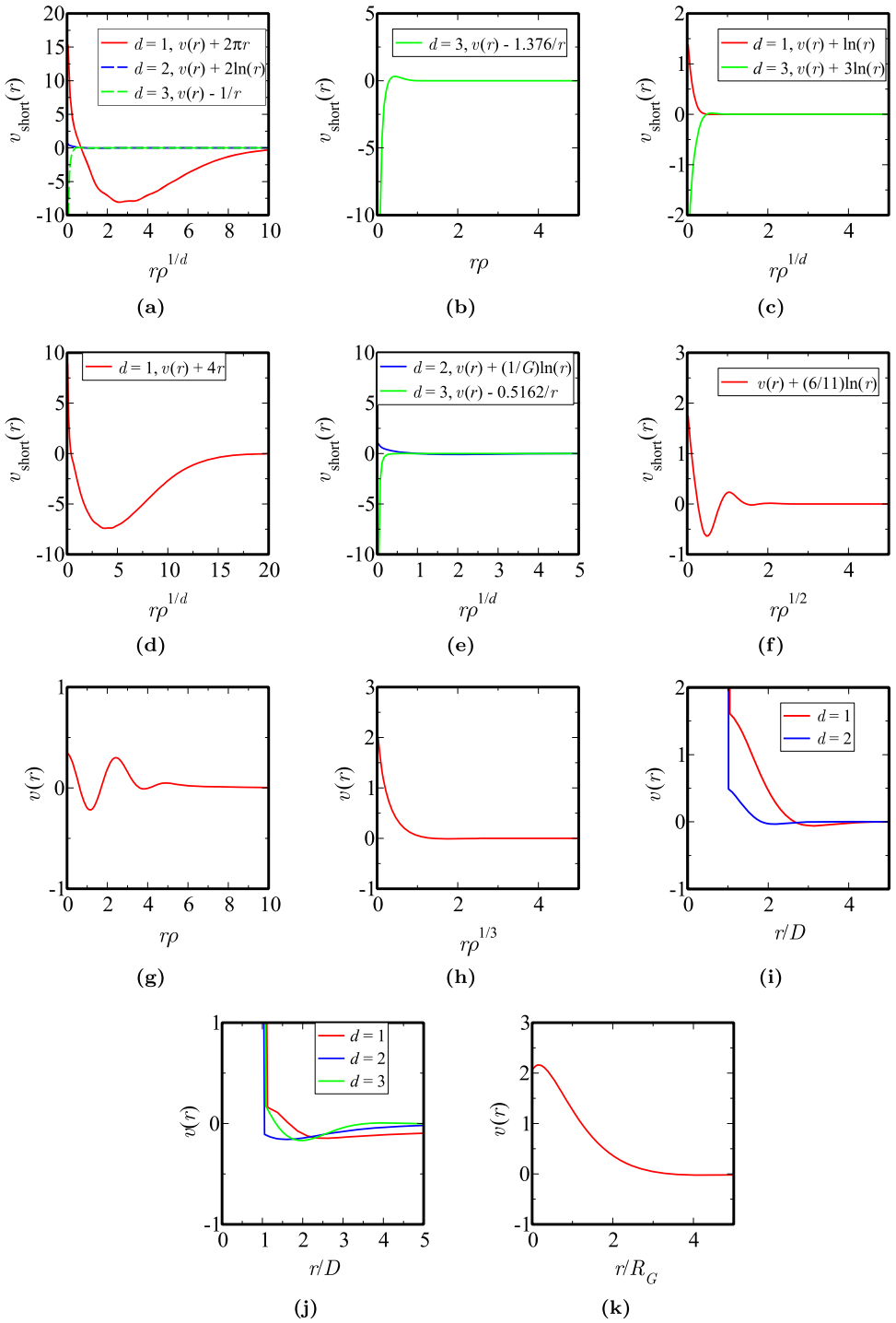


FIG. 12. (a) Short-ranged part of the effective pair potentials (B1)–(B3) for the 1D, 2D, and 3D Gaussian pair statistics. (b) Short-ranged part of the effective pair potential (B5) for the 3D OCP pair statistics. (c) Short-ranged part of the effective potentials (B6) and (B7) for 1D and 3D Fourier dual of OCP pair statistics. (d) Short-ranged part of the effective potential (B8) for the 1D hyperbolic secant $g_2(r)$. (e) Short-ranged part of the effective potentials, Eqs. (B9) and (B10), for 2D and 3D hyperbolic secant $g_2(r)$, respectively. (f) Short-ranged part of the effective potential (B11) for the 2D Gaussian-damped polynomial pair statistics. (g) Effective potentials (B12) for the 1D hyposurficial Hermite–Gaussian $g_2(r)$ with $\lambda = 1/20$. (h) Effective potential (B13) for the 3D hyposurficial state. (i) Effective potentials (B14) and (B15) for the 1D and 2D "ghost" RSA. (j) Effective potentials (B16)–(B18) for 1D, 2D, and 3D antihyperuniform states. (k) Effective potentials for a 3D polymer model with the total correlation function (33) at $\rho = 0.5$.

31 January 2024 15:02:42

Published under an exclusive license by AIP Publishing

to describe the intermolecular forces of star polymers.[108] We also find that the oscillatory soft potentials in the cases of polynomial-damped pair statistics can be achieved by "sticky" macromolecules such as DNA-coated nanoparticles[90] and that the combination of hard core and soft repulsion in the interactions for the ghost RSA packings can be found in colloidal suspensions of highly charged nanoparticles.[95]

The excellent agreement between the designed and simulated pair statistics in all cases studied in this work demonstrates the power of our inverse procedure to tackle realizability problems. It can be applied to study many prescribed pair functions at different densities and temperatures other than those explicitly shown in this work, provided that $g_2(r)$ and $S(k)$ at least meet necessary nonnegativity conditions. For example, we have shown that anti-hyperuniform critical-point systems can be designed that do not belong to the Ising universality class. Remarkably, 1D critical-point states, which are impossible in 1D models with Ising-like short-ranged interactions, can be achieved as a result of the long-ranged pair potentials determined via our inverse procedure. Knowledge of the critical point is essential in the construction of phase diagrams for fluids.[40] Previous studies on critical points typically utilized the direct approach of statistical mechanics, i.e., simulations with known potentials. Our inverse approach in generating antihyperuniform systems of different universality classes can significantly accelerate the exploration of the phase diagram and the fabrication of systems with fractal-like structures. One can also systematically study the realizability of $g_2(r)$ with different asymptotic decay rates at large r, including power-law, exponential, and super-exponential rates. It is known that the decay behavior of $g_2(r)$ for a fluid determines the Fisher–Widom line that separates liquid-like and gas-like behaviors in the supercritical region.[38,109] Thus, $g_2(r)$ with prescribed decay rates may enable one to create many-particle systems with desired phase behaviors.

Another important future project is to target disordered hyperuniform structure factors with $\alpha \geq 3$ for their potential optical applications.[81] Furthermore, we remark that the pair functions in Table I can be used as basis functions to create new designs at unit density, i.e.,

$$g_2^*(r) = \Sigma_{i=1}^n \lambda_i g_{2,i}(r), \quad 0 \leq \lambda_i \leq 1, \Sigma_i^n \lambda_i = 1. \tag{39}$$

Equation (39) is expected to be realizable because it is realizable in all of the extreme cases where $\lambda_i = 1$. For example, in quantum-mechanical systems, the form (39) may be achieved by a quantum superposition of individual states with pair correlation functions given by $g_{2,i}(r)$. Finally, note that if a given $g_2(r)$ is realizable at $\rho = 1$, then it is also realizable at all lower densities because the realizable density range for a given $g_2(r)$ is always a continuous interval.[110]

Because pair statistics based on our designed functions exhibit distinctly different translational order and self-diffusivity, they can have potential applications in the design of many-particle systems with tailored mass transport properties. Importantly, while Fig. 11 shows discrete values of τ and $\mathcal{D}$ for the 3D models in Table I, values between the plotted points can be achieved by linear combinations of our pair functions in the form of Eq. (39), and their corresponding potentials can be readily determined via our inverse procedure. Thus, one can flexibly design pair functions that yield a continuous spectrum of τ and $\mathcal{D}$ values. In the context of diffusion-controlled reactions, the designed pair statistics would guide the fabrication of nanoparticles, micelles, or vesicles loaded with reactants or catalysts to achieve desired reaction rates.[111,112] Moreover, since our procedure can realize a wide range of short- and long-range orders, the equilibrium states can be modified into multi-phase media with tailored long-time diffusion spreadability[113] for controlled drug delivery purposes.[114]

Our study also has important implications for the Zhang–Torquato conjecture, which states that any realizable set of pair statistics, whether from a nonequilibrium or equilibrium system, can be achieved by equilibrium systems involving up to two-body interactions.[32] We have previously tested this conjecture by accurately determining effective potentials for various nonequilibrium pair statistics, including the unit-step function $g_2(r)$ from zero density to the dimension-dependent maximum realizable densities across the first three space dimensions,[24] 3D ghost RSA,[24] "cloaked" uniformly randomized lattices,[33] and perfect glasses and critical absorbing states.[65] The realizability of all the prescribed pair statistics in this study lends further support to this conjecture. In the future, it is important to further test this conjecture with other nonequilibrium pair statistics, including those of quantum states.[45]

SUPPLEMENTARY MATERIAL

The supplementary material provides a plot of the intermolecular force $dv(r)/dr$ corresponding to the effective pair potentials for our 3D hyperuniform models.

ACKNOWLEDGMENTS

This work was supported in part by the National Science Foundation Grant No. CBET-2133179 and the U.S. Army Research Office 171 under Cooperative Agreement No. W911NF-22-2-0103.

AUTHOR DECLARATIONS

Conflict of Interest

The authors have no conflicts to disclose.

Author Contributions

S.T. conceived of the project and research questions; H.W. and S.T. performed the research and H.W. carried out all numerical calculations; and H.W. and S.T. wrote the paper.

Haina Wang: Data curation (lead); Formal analysis (lead); Investigation (equal); Methodology (equal); Writing – original draft (equal); Writing – review & editing (equal). **Salvatore Torquato**: Conceptualization (lead); Investigation (equal); Methodology (equal); Writing – original draft (equal); Writing – review & editing (equal).

DATA AVAILABILITY

Analytical pair functions that are known to be realizable, including the ones in this and previous studies, are available in the PairFunctions repository, Ref. 115.

31 January 2024 15:02:42

Published under an exclusive license by AIP Publishing

APPENDIX A: STRUCTURE FACTORS FOR ANTIHYPERUNIFORM STATES

- 1D case:

$$S(k) = 1 + \phi A\sqrt{\frac{2\pi}{kD}}\left(-2\text{FresnelC}\left(\sqrt{\frac{2kD}{\pi}}\right) + 1\right) - 2\phi\frac{\sin(k)}{kD}, \tag{A1}$$

where we use $\phi = 0.2, A = 0.1$ in this work.

- 2D case:

$$S(k) = 1 - 16A\phi_1 F_2\left(\frac{1}{4}; 1, \frac{5}{4}; -\frac{k^2}{4}\right) + \frac{4\sqrt{2}A\phi\Gamma\left(\frac{1}{4}\right)}{\sqrt{k}\Gamma\left(\frac{3}{4}\right)} - \frac{8\phi J_1(k)}{k}, \tag{A2}$$

where we use $\phi = 0.1, A = 0.3$.

- 3D case:

$$S(k) = 1 + \frac{24\sqrt{2\pi}A\phi - 48\sqrt{2\pi}A\phi\text{FresnelC}\left(\sqrt{\frac{2kD}{\pi}}\right)}{\sqrt{kD}} + \frac{48A\phi\sin(kD)}{kD} - \frac{24\phi\sin(kD)}{(kD)^3} + \frac{24\phi\cos(kD)}{(kD)^2}, \tag{A3}$$

where we use $\phi = 0.1, A = 0.25$.

APPENDIX B: EFFECTIVE POTENTIALS

- 1D Gaussian pair statistics:

$$v(r) = -2\pi r - \varepsilon_1^{(1)}\exp\left(-(r/\sigma_1)^2\right)(\ln(r) + \varepsilon_1^{(2)}) + \sum_{j=2}^{4}\varepsilon_j\cos\left(r/\sigma_j^{(1)} + \theta_j\right)\exp\left(-(r/\sigma_j^{(2)})^2\right), \tag{B1}$$

where the optimized values of the parameters are given in Table II.

- 2D Gaussian pair statistics:

$$v(r) = -2\ln(r). \tag{B2}$$

- 3D Gaussian pair statistics:

$$v(r) = (1/r)\left(1 - \exp\left(-(r/\sigma_1)^2\right)\right) - \varepsilon_2\exp\left(-(r/\sigma_2)^2\right)\ln(r), \tag{B3}$$

where $\sigma_1 = 0.4672, \varepsilon_2^{(1)} = 1.877, \sigma_2 = 0.6176$.

- 1D OCP pair statistics:

$$v(r) = -2r - \varepsilon_1^{(1)}\exp\left(-(r/\sigma_1)^2\right)(\ln(r) + \varepsilon_1^{(2)}) + \sum_{j=2}^{3}\varepsilon_j\cos\left(r/\sigma_j^{(1)} + \theta_j\right)\exp\left(-(r/\sigma_j^{(2)})^2\right), \tag{B4}$$

where the optimized values of the parameters are given in Table III.

- 3D OCP pair statistics:

$$v(r) = \frac{9}{2}\frac{3^{5/6}\Gamma\left(\frac{4}{3}\right)}{2^{2/3}\pi^{4/3}r}\left(1 - \exp\left(-(r/\sigma_2)^2\right)\right) - \varepsilon_2\exp\left(-(r/\sigma_1)^2\right)\ln(r), \tag{B5}$$

where $\sigma_1 = 0.4149, \varepsilon_2 = 3.008, \sigma_2 = 0.5624$.

- Fourier dual of 1D OCP pair statistics:

$$v(r) = -\ln(r)\left(1 - \exp\left(-(r/\sigma_1)^2\right)\right) - \varepsilon_2\exp\left(-(r/\sigma_2)^2\right)\ln(r), \tag{B6}$$

where $\sigma_1 = 0.2331, \varepsilon_2 = 1.375, \sigma_2 = 0.2331$.

- Fourier dual of 3D OCP pair statistics:

$$v(r) = -3\ln(r) + \ln\left(r/\sigma_1^{(1)}\right)\exp\left(-(r/\sigma_1^{(2)})^2\right), \tag{B7}$$

where $\sigma_1^{(1)} = 0.4791$ and $\sigma_1^{(2)} = 0.4038$.

- 1D hyperbolic secant function $g_2(r)$:

$$v(r) = -4r - \varepsilon_1^{(1)}\exp\left(-(r/\sigma_1)^2\right)(\ln(r) + \varepsilon_1^{(2)}) + \sum_{j=2}^{3}\varepsilon_j\cos\left(r/\sigma_j^{(1)} + \theta_j\right)\exp\left(-(r/\sigma_j^{(2)})^2\right), \tag{B8}$$

TABLE II. Parameters of the effective pair potential (B1) for 1D Gaussian pair statistics.

$\varepsilon_1^{(1)}$	7.368	ε_2	20.15	ε_3	−0.2078	ε_4	0.020 70
σ_1	5.433	$\sigma_2^{(1)}$	2.311	$\sigma_3^{(1)}$	0.1564	$\sigma_3^{(1)}$	$1/(2\pi)$
$\varepsilon_1^{(2)}$	0.3824	θ_2	4.536	θ_3	2.911	θ_4	0
		$\sigma_2^{(2)}$	0.7983	$\sigma_3^{(2)}$	3.305	$\sigma_4^{(2)}$	86.07

TABLE III. Parameters of the effective pair potential (B4) for the 1D OCP pair statistics.

$\varepsilon_1^{(1)}$	1.727	ε_2	35.72	ε_3	−8.917
σ_1	14.22	$\sigma_2^{(1)}$	6.501	$\sigma_3^{(1)}$	1.915
$\varepsilon_1^{(2)}$	1.947	θ_2	4.438	θ_3	3.520
		$\sigma_2^{(2)}$	1.560	$\sigma_3^{(2)}$	1.393

31 January 2024 15:02:42

Published under an exclusive license by AIP Publishing

TABLE IV. Parameters of the effective pair potential (B8) for the 1D hyperbolic secant function $g_2(r)$.

$\varepsilon_1^{(1)}$	5.172	ε_2	22.28	ε_3	−0.062 83
σ_1	7.728	$\sigma_2^{(1)}$	8.071	$\sigma_3^{(1)}$	0.1610
$\varepsilon_1^{(2)}$	0.4883	θ_2	4.517	θ_3	3.241
		$\sigma_2^{(2)}$	0.6085	$\sigma_3^{(2)}$	4.170

TABLE V. Parameters of the effective pair potential (B11) for the 2D Gaussian-damped polynomial pair statistics.

σ_1	1.081	$\sigma_3^{(1)}$	0.1843
ε_2	0.8532	θ	0.3920
σ_2	0.4884	$\sigma_3^{(2)}$	0.9862
ε_3	0.7009		

where the optimized values of the parameters are given in Table IV.

- 2D hyperbolic secant function $g_2(r)$:

$$v(r) = -\frac{1}{G}\ln(r)\left(1-\exp\left(-\left(\frac{r}{\sigma_1}\right)^2\right)\right) - \varepsilon_2 \exp\left(-\left(\frac{r}{\sigma_2}\right)^2\right)\ln(r), \tag{B9}$$

where $\sigma_1 = 2.269, \varepsilon_2 = 1.367, \sigma_2 = 2.269$.

- 3D hyperbolic secant function $g_2(r)$:

$$v(r) = \frac{3\sqrt[3]{\frac{2}{\pi}}}{5r}(1-\exp(-(r/\sigma_1)^2)) - \varepsilon_2 \exp(-(r/\sigma_2)^2)\ln(r), \tag{B10}$$

where $\sigma_1 = 0.1557, \varepsilon_2 = 1.922, \sigma_2 = 0.1174$.

- 2D Gaussian-damped polynomial pair statistics:

$$v(r) = -\frac{6}{11}\ln(r)\left(1-e^{-\left(\frac{r}{\sigma_1}\right)^2}\right) - \varepsilon_2 \ln(r) \times e^{-\left(\frac{r}{\sigma_2}\right)^2} + \varepsilon_3 \cos\left(\frac{r}{\sigma_3^{(1)}}+\theta\right)e^{-\left(\frac{r}{\sigma_3^{(2)}}\right)^2}, \tag{B11}$$

where the optimized values of the parameters are given in Table V.

- 1D Hermite–Gaussian pair statistics with $\lambda = 1/20$:

$$v(r) = \sum_{j=1}^{2} \varepsilon_j \cos(r/\sigma_j^{(1)} + \theta_j)\exp(-r/\sigma_j^{(2)}) + \varepsilon_3 \exp(-r/\sigma_3), \tag{B12}$$

where the optimized values of the parameters are given in Table VI.

- 3D hyposurficial state:

$$v(r) = \sum_{j=1}^{2} \varepsilon_j \exp(-r/\sigma_j) + \varepsilon_3 \exp(-((r-\sigma_3^{(1)})/\sigma_3^{(2)})^2), \tag{B13}$$

where the optimized values of the parameters are given in Table VII.

- 1D ghost RSA:

$$v(r) = \begin{cases} \infty, & r < 0.5, \\ \varepsilon_1 \exp(-(r/\sigma_1^{(1)})^2)\cos(r/\sigma_1^{(2)} + \theta), & r \geq 0.5, \end{cases} \tag{B14}$$

where $\varepsilon_1 = -2.341$, $\sigma_1^{(1)} = 0.9045$, $\sigma_1^{(2)} = -0.4406$, $\theta = -1.686$.

- 2D ghost RSA:

$$v(r) = \begin{cases} \infty, & r < 1/\sqrt{\pi}, \\ \varepsilon_1 \exp(-(r/\sigma_1^{(1)})^2)\cos(r/\sigma_1^{(2)} + \theta), & r \geq 1/\sqrt{\pi}, \end{cases} \tag{B15}$$

where $\varepsilon_1 = 0.8107, \sigma_1^{(1)} = 0.7860, \sigma_1^{(2)} = 0.2867, \theta = -1.982$.

- 1D antihyperuniform state:

$$v(r) = \begin{cases} \infty, & r < D, \\ -\varepsilon_1/\sqrt{r/D} + \varepsilon_2 \exp(-(r/D-1)/\sigma_2) + \varepsilon_3 \exp(-((r/D-1)/\sigma_3)^2), & r > D, \end{cases} \tag{B16}$$

where $\varepsilon_1 = 0.3311, \varepsilon_2 = 0.0552, \sigma_2 = 70.21, \varepsilon_3 = 0.4299, \sigma_3 = 0.7560$.

- 2D antihyperuniform state:

$$v(r) = \begin{cases} \infty, & r < D, \\ -\varepsilon_1/(r/D)^{3/2} + \varepsilon_2 \exp(-(r/D-1)/\sigma_2^{(1)})\cos(r/(D\sigma_2^{(2)}) + \theta), & r > D, \end{cases} \tag{B17}$$

where $\varepsilon_1 = 0.1483, \varepsilon_2 = 1.647, \sigma_2 = 0.7530, \sigma_2^{(2)} = -4.120, \theta = 4.987$.

- 3D antihyperuniform state:

$$v(r) = \begin{cases} \infty, & r < D, \\ -\varepsilon_1/(r/D)^{5/2} + \varepsilon_2 \exp(-(r/D-1)/\sigma_2^{(1)})\cos(r/(D\sigma_2^{(2)}) + \theta), & r > D, \end{cases} \tag{B18}$$

where $\varepsilon_1 = 0.2100, \varepsilon_2 = 0.6116, \sigma_2 = 0.7927, \sigma_2^{(2)} = -0.5982, \theta = 7.203$.

31 January 2024 15:02:42

Published under an exclusive license by AIP Publishing

- 3D hypothetical polymer motivated by the PRISM model:

$$v(r) = \varepsilon_1 \exp\left(-(r/\sigma_1^{(1)})\right) \cos\left(r/\sigma_1^{(2)} + \theta\right) + \varepsilon_2 \exp\left(-r/\sigma_2\right), \tag{B19}$$

where $\varepsilon_1 = 3.635, \sigma_1^{(1)} = 0.9891, \sigma_1^{(2)} = 1.663, \theta = -0.4998, \varepsilon_2 = -1.133, \sigma_2 = 0.3150$.

TABLE VI. Parameters of the effective pair potential (B12) for the 1D Hermite–Gaussian pair statistics with $\lambda = 1/20$.

ε_1	0.4143	ε_2	3.174	ε_3	0.2663
$\sigma_1^{(1)}$	0.4250	$\sigma_2^{(1)}$	14.24	σ_3	2.392
θ_1	0.2047	θ_2	4.609		
$\sigma_1^{(2)}$	2.829	$\sigma_2^{(2)}$	1.544		

TABLE VII. Parameters of the effective pair potential (B13) for the 3D hyposurficial state.

ε_1	1.646	ε_3	−0.1241
σ_1	0.4070	$\sigma_3^{(1)}$	0.2020
ε_2	0.8742	$\sigma_3^{(2)}$	1.312
σ_2	0.8884		

REFERENCES

[1] F. J. Dyson, "Statistical theory of the energy levels of complex systems. I," J. Math. Phys. **3**, 140–156 (1962).
[2] R. P. Feynman, *Statistical mechanics* (Westview Press, Boulder, Colorado, 1998).
[3] K. Van Workum and J. F. Douglas, "Symmetry, equivalence, and molecular self-assembly," Phys. Rev. E **73**, 031502 (2006).
[4] J. P. Hansen and I. R. McDonald, *Theory of Simple Liquids* (Academic Press, New York, 1986).
[5] Y. Jiao, T. Lau, H. Hatzikirou, M. Meyer-Hermann, J. C. Corbo, and S. Torquato, "Avian photoreceptor patterns represent a disordered hyperuniform solution to a multiscale packing problem," Phys. Rev. E **89**, 022721 (2014).
[6] D. Hexner and D. Levine, "Hyperuniformity of critical absorbing states," Phys. Rev. Lett. **114**, 110602 (2015).
[7] S. Torquato, *Random Heterogeneous Materials: Microstructure* (Springer-Verlag, New York, 2002).
[8] S. Torquato, Z. W. Wang, and C. Holm, "Swimming in circles can lead to exotic hyperuniform states of active living matter," Proc. Natl. Acad. Sci. **118**, e2100493118 (2021).
[9] D. M. Nicholson, C. Y. Gao, M. T. McDonnell, C. C. Sluss, and D. J. Keffer, "Entropy pair functional theory: Direct entropy evaluation spanning phase transitions," Entropy **23**, 234 (2021).
[10] J.-L. Bretonnet, "Self-diffusion coefficient of dense fluids from the pair correlation function," J. Chem. Phys. **117**, 9370–9373 (2002).
[11] W. P. Krekelberg, M. J. Pond, G. Goel, V. K. Shen, J. R. Errington, and T. M. Truskett, Phys. Rev. E **80**, 061205 (2009).
[12] W. P. Krekelberg, T. Kumar, J. Mittal, J. R. Errington, and T. M. Truskett, "Anomalous structure and dynamics of the Gaussian-core fluid," Phys. Rev. E **79**, 031203 (2009).
[13] J. G. Kirkwood, F. P. Buff, and M. S. Green, "The statistical mechanical theory of transport processes. III. The coefficients of shear and bulk viscosity of liquids," J. Chem. Phys. **17**, 988–994 (2004).
[14] N. Gnan, C. Maggi, T. B. Schrøder, and J. C. Dyre, "Predicting the effective temperature of a glass," Phys. Rev. Lett. **104**, 125902 (2010).
[15] S. Torquato, "Diffusion spreadability as a probe of the microstructure of complex media across length scales," Phys. Rev. E **104**, 054102 (2021).
[16] S. Torquato, A. Scardicchio, and C. E. Zachary, "Point processes in arbitrary dimension from fermionic gases, random matrix theory, and number theory," J. Stat. Mech.: Theory Exp. **2008**, P11019.
[17] A. Soshnikov, Russ. Math. Surv. **55**, 923–975 (2000).
[18] J. B. Hough, M. Krishnapur, Y. Peres, and B. Virág, *Zeros of Gaussian Analytic Functions and Determinantal Point Processes* (American Mathematical Society, Providence, RI, 2009), Vol. 51.
[19] O. Costin and J. Lebowitz, "On the construction of particle distributions with specified single and pair densities," J. Phys. Chem. B **108**, 19614–19618 (2004).
[20] B. Jancovici, "Exact results for the two-dimensional one-component plasma," Phys. Rev. Lett. **46**, 386–388 (1981).
[21] These include d-dimensional ground-state free fermions (Refs. 2 and 16), eigenvalues for certain random matrices (Refs. 1, 17, and 18), 1D Lorentzian $g2(r)$ [19], and 2D Ginibre ensemble (Ref. 20).
[22] F. Zernike and J. A. Prins, "Die Beugung von Röntgenstrahlen in Flüssigkeiten als Effekt der Molekülanordnung," Z. Phys. A: Hadrons Nucl. **41**, 184–194 (1927).
[23] S. Torquato and F. H. Stillinger, "Exactly solvable disordered sphere-packing model in arbitrary-dimensional Euclidean spaces," Phys. Rev. E **73**, 031106 (2006).
[24] H. Wang, F. H. Stillinger, and S. Torquato, "Realizability of iso-g_2 processes via effective pair interactions," J. Chem. Phys. **157**, 224106 (2022).
[25] S. Axelrod, D. Schwalbe-Koda, S. Mohapatra, J. Damewood, K. P. Greenman, and R. Gómez-Bombarelli, "Learning matter: Materials design with machine learning and atomistic simulations," Acc. Mater. Res. **3**, 343–357 (2022).
[26] S. Torquato and F. H. Stillinger, "Controlling the short-range order and packing densities of many-particle systems," J. Phys. Chem. B **106**, 8354–8359 (2002), Erratum **106**, 11406 (2002).
[27] S. Torquato and F. H. Stillinger, Exp. Math. **15**, 307–331 (2006).
[28] M. Yamada, "Geometrical study of the pair distribution function in the many-body problem," Prog. Theor. Phys. **25**, 579–594 (1961).
[29] A. Lenard, "Correlation functions and the uniqueness of the state in classical statistical mechanics," Commun. Math. Phys. **30**, 35–44 (1973).
[30] T. Kuna, J. L. Lebowitz, and E. R. Speer, "Necessary and sufficient conditions for realizability of point processes," Ann. Appl. Probab. **21**, 1253–1281 (2011).
[31] R. Lachieze-Rey and I. Molchanov, "Regularity conditions in the realisability problem with applications to point processes and random closed sets," Ann. Appl. Prob. **25**, 116–149 (2015).
[32] G. Zhang and S. Torquato, "Realizable hyperuniform and nonhyperuniform particle configurations with targeted spectral functions via effective pair interactions," Phys. Rev. E **101**, 032124 (2020).
[33] S. Torquato and H. Wang, "Precise determination of pair interactions from pair statistics of many-body systems in and out of equilibrium," Phys. Rev. E **106**, 044122 (2022).
[34] S. Torquato and F. H. Stillinger, "Local density fluctuations, hyperuniformity, and order metrics," Phys. Rev. E **68**, 041113 (2003).
[35] S. Torquato, Phys. Rep. **745**, 1–95 (2018).
[36] C. E. Zachary and S. Torquato, "Hyperuniformity in point patterns and two-phase random heterogeneous media," J. Stat. Mech.: Theory Exp. **2009**, P12015.
[37] S. Torquato, "Structural characterization of many-particle systems on approach to hyperuniform states," Phys. Rev. E **103**, 052126 (2021).
[38] B. Widom, "Equation of state in the neighborhood of the critical point," J. Chem. Phys. **43**, 3898–3905 (1965).
[39] L. P. Kadanoff, "Scaling laws for ising models near T_c," Phys. Phys. Fiz. **2**, 263–272 (1966).

31 January 2024 15:02:42

Published under an exclusive license by AIP Publishing

[40]M. E. Fisher, "The theory of equilibrium critical phenomena," Rep. Prog. Phys. **30**, 615 (1967).
[41]K. G. Wilson and J. Kogut, "The renormalization group and the ε expansion ϵ expansion," Phys. Rep. **12**, 75–199 (1974).
[42]J. J. Binney, N. J. Dowrick, A. J. Fisher, and M. E. J. Newman, *The Theory of Critical Phenomena: An Introduction to the Renormalization Group* (Oxford University Press, Oxford, England, 1992).
[43]B. B. Mandelbrot, *The Fractal Geometry of Nature* (W. H. Freeman, New York, 1982).
[44]E. C. Oğuz, J. E. S. Socolar, P. J. Steinhardt, and S. Torquato, "Hyperuniformity and anti-hyperuniformity in one-dimensional substitution tilings," Acta Crystallogr., Sect. A: Found. Adv. **75**, 3–13 (2019).
[45]S. Torquato and F. H. Stillinger, "New duality relations for classical ground states," Phys. Rev. Lett. **100** 020602 (2008).
[46]S. Torquato, C. E. Zachary, and F. H. Stillinger, Soft Matter **7**, 3780 (2011).
[47]S. Torquato, "Reformulation of the covering and quantizer problems as ground states of interacting particles," Phys. Rev. E **82**, 056109 (2010).
[48]Here, ${}_pF_q(a_1,\ldots,a_p;b_1,\ldots,b_q;z)$ is the generalized hypergeometric function and $\mathrm{ber}_v(z)$ is the Kelvin function.
[49]Here, $G = 0.915\ldots$ is Catalan's constant.
[50]Here, λ is a parameter controlling the amplitude of oscillations in the pair statistics. The condition that $S(k) \geq 0$ for all k implies that $\lambda \leq \exp\left(\sqrt{11/2}/2 + 7/4\right)/\left(8\left(\sqrt{22}+4\right)\sqrt{2\pi}\right) = 0.1067\ldots$.
[51]Here, $r^* = (4\pi)^{1/3} r$ and $k^* = (4\pi)^{-1/3} k$.
[52]Here, Ci is the cosine integral and Si is the sine integral.
[53]Here $r^* = \sqrt{\pi} r$.
[54]Here, D is the hard-core diameter and $A+1$ is the peak height of $g_2(r)$ as $r \to D^+$.
[55]K. S. Schweizer and J. G. Curro, "Integral equation theories of the structure, thermodynamics, and phase transitions of polymer fluids," in *Advances in Chemical Physics* (John Wiley & Sons, Ltd., 1997), pp. 1–142.
[56]G. Yatsenko, E. J. Sambriski, M. A. Nemirovskaya, and M. Guenza, "Analytical soft-core potentials for macromolecular fluids and mixtures," Phys. Rev. Lett. **93**, 257803 (2004).
[57]S. Torquato, G. Zhang, and F. H. Stillinger, "Ensemble theory for stealthy hyperuniform disordered ground states," Phys. Rev. X **5**, 021020 (2015).
[58]R. L. Henderson, "A uniqueness theorem for fluid pair correlation functions," Phys. Lett. A **49**, 197–198 (1974).
[59]R. D. Neidinger, SIAM Rev. **52**, 545–563 (2010).
[60]A. B. Norgaard, J. Ferkinghoff-Borg, and K. Lindorff-Larsen, "Experimental parameterization of an energy function for the simulation of unfolded proteins," Biophys. J. **94**, 182–192 (2008).
[61]J. P. Hansen, "Statistical mechanics of dense ionized matter. I. Equilibrium properties of the classical one-component plasma," Phys. Rev. A **8**, 3096–3109 (1973).
[62]R. C. Gann, S. Chakravarty, and G. V. Chester, "Monte Carlo simulation of the classical two-dimensional one-component plasma," Phys. Rev. B **20**, 326–344 (1979).
[63]P. P. Ewald, Ann. Phys. **369**, 253–287 (1921).
[64]D. C. Liu and J. Nocedal, "On the limited memory BFGS method for large scale optimization," Math. Program. **45**, 503–528 (1989).
[65]H. Wang and S. Torquato, Soft Matter **19**, 550–564 (2023).
[66]J. Revels, M. Lubin, and T. Papamarkou, "Forward-mode automatic differentiation in Julia," arXiv:1607.07892 [cs.MS] (2016).
[67]A. K. Soper, "Empirical potential Monte Carlo simulation of fluid structure," Chem. Phys. **202**, 295–306 (1996).
[68]L. S. Ornstein and F. Zernike, "Accidental deviations of density and opalescence at the critical point of a single substance," Proc. Akad. Sci. (Amsterdam) **17**, 793–806 (1914).
[69]P. Flory and A. Bueche, "Theory of light scattering by polymer solutions," J. Polym. Sci. **27**, 219–229 (1958).
[70]J. Koplik, H. Levine, and A. Zee, "Viscosity renormalization in the Brinkman equation," Phys. Fluids **26**, 2864–2870 (1983).
[71]N. Becker, A. Rosa, and R. Everaers, Eur. Phys. J. E **32**, 53–69 (2010).
[72]F. H. Stillinger, "Phase transitions in the Gaussian core system," J. Chem. Phys. **65**, 3968 (1976).
[73]A. A. Louis, P. G. Bolhuis, and J. P. Hansen, "Mean-field fluid behavior of the Gaussian core model," Phys. Rev. E **62**, 7961–7972 (2000).
[74]C. E. Zachary, F. H. Stillinger, and S. Torquato, "Gaussian core model phase diagram and pair correlations in high Euclidean dimensions," J. Chem. Phys. **128**, 224505 (2008).
[75]S. Prestipino, F. Saija, and P. V. Giaquinta, "Phase diagram of the Gaussian-core model," Phys. Rev. E **71**, 050102 (2005).
[76]M. Baus and J.-P. Hansen, "Statistical mechanics of simple Coulomb systems," Phys. Rep. **59**, 1–94 (1980).
[77]F. Müller-Plathe, ChemPhysChem **3**, 754–769 (2002).
[78]E. Slyk, T. Skora, and S. Kondrat, Soft Matter **18**, 5366–5370 (2022).
[79]S. Kragset, A. Sudbø, and F. S. Nogueira, "Metal-insulator transition in two- and three-dimensional logarithmic plasmas," Phys. Rev. Lett. **92**, 186403 (2004).
[80]K. Børkje, S. Kragset, and A. Sudbø, "Instanton correlators and phase transitions in two- and three-dimensional logarithmic plasmas," Phys. Rev. B **71**, 085112 (2005).
[81]S. Torquato and J. Kim, Phys. Rev. X **11**, 021002 (2021).
[82]M. Faliva and M. G. Zoia, "A distribution family bridging the Gaussian and the Laplace laws, Gram–Charlier expansions, kurtosis behaviour, and entropy features," Entropy **19**, 149 (2017).
[83]C. N. Likos, H. Löwen, M. Watzlawek, B. Abbas, O. Jucknischke, J. Allgaier, and D. Richter, "Star polymers viewed as ultrasoft colloidal particles," Phys. Rev. Lett. **80**, 4450–4453 (1998).
[84]J. Stellbrink, J. Allgaier, M. Monkenbusch, D. Richter, A. Lang, C. Likos, M. Watzlawek, H. Löwen, G. Ehlers, and P. Schleger, "Neither Gaussian chains nor hard spheres - Star polymers seen as ultrasoft colloids," *Trends in Colloid and Interface Science XIV* (Springer, Berlin & Heidelberg, 2000), pp. 88–92.
[85]S. Torquato, J. D. Beasley, and Y. C. Chiew, "Two-point cluster function for continuum percolation," J. Chem. Phys. **88**, 6540–6547 (1988).
[86]R. Xu and D. WunschII, "Survey of clustering algorithms," IEEE Trans. Neural Networks **16**, 645–678 (2005).
[87]J. P. Donley, J. J. Rajasekaran, and A. J. Liu, "Density pair correlation functions for molecular liquids: Approximations for polymers," J. Chem. Phys. **109**, 10499–10512 (1998).
[88]A. Yethiraj, H. Fynewever, and C.-Y. Shew, "Density functional theory for pair correlation functions in polymeric liquids," J. Chem. Phys. **114**, 4323–4330 (2001).
[89]J. Wilhelm and E. Frey, "Radial distribution function of semiflexible polymers," Phys. Rev. Lett. **77**, 2581–2584 (1996).
[90]B. M. Mladek, J. Fornleitner, F. J. Martinez-Veracoechea, A. Dawid, and D. Frenkel, Soft Matter **9**, 7342–7355 (2013).
[91]A. Kumar and V. Molinero, J. Phys. Chem. Lett. **8**, 5053–5058 (2017).
[92]F. Martelli, S. Torquato, N. Giovambattista, and R. Car, "Large-scale structure and hyperuniformity of amorphous ices," Phys. Rev. Lett. **119**, 136002 (2017).
[93]A. Reńyi, "On a one-dimensional problem concerning random space filling," Sel. Trans. Math. Stat. Prob. **4**, 203–218 (1963).
[94]B. Widom, "Random sequential addition of hard spheres to a volume," J. Chem. Phys. **44**, 3888–3894 (1966).
[95]J. Liu and E. Luijten, "Stabilization of colloidal suspensions by means of highly charged nanoparticles," Phys. Rev. Lett. **93**, 247802 (2004).
[96]C. Wissel, Oecologia **65**, 101–107 (1984).
[97]F. J. Dyson, "Existence of a phase-transition in a one-dimensional Ising ferromagnet," Commun. Math. Phys. **12**, 91–107 (1969).
[98]B. A. Cipra, "An introduction to the Ising model," Am. Math. Mon. **94**, 937–959 (1987).
[99]The metric τ can still be used to analyze crystals by examining its growth with the system size for finite configurations (Ref. 33).
[100]O. H. E. Philcox and S. Torquato, "Disordered heterogeneous universe: Galaxy distribution and clustering across length scales," Phys. Rev. X **13**, 011038 (2023).
[101]Y. Rosenfeld, "A quasi-universal scaling law for atomic transport in simple fluids," J. Phys.: Condens. Matter **11**, 5415 (1999).

31 January 2024 15:02:42

Published under an exclusive license by AIP Publishing

[102]E. Lomba, J.-J. Weis, and S. Torquato, "Disordered hyperuniformity in two-component nonadditive hard-disk plasmas," Phys. Rev. E **96**, 062126 (2017).
[103]M. Dzugutov, "A universal scaling law for atomic diffusion in condensed matter," Nature **381**, 137–139 (1996).
[104]G. Czarnecki, M. R. Dudek, A. Pekalski, and J. Cislo, "Tracer diffusion of particles with soft-core interactions studied by Monte Carlo simulations," J. Phys. A: Math. Gen. **29**, 3367 (1996).
[105]Z. Ma and S. Torquato, "Random scalar fields and hyperuniformity," J. Appl. Phys. **121**, 244904 (2017).
[106]A. Chremos and J. F. Douglas, "Hidden hyperuniformity in soft polymeric materials," Phys. Rev. Lett. **121**, 258002 (2018).
[107]These include Gaussian pair statistics, OCP and its Fourier dual, and the hyperbolic secant $g_2(r)$.
[108]A. J. Archer, C. N. Likos, and R. Evans, "Binary star-polymer solutions: Bulk and interfacial properties," J. Phys.: Conds. Matter **14**, 12031 (2002).
[109]M. E. Fisher and B. Wiodm, "Decay of correlations in linear systems," J. Chem. Phys. **50**, 3756–3772 (2003).
[110]F. H. Stillinger and S. Torquato, "Realizability issues for iso-$g^{(2)}$processes," Mol. Phys. **103**, 2943–2949 (2005).
[111]N. Wakao and J. Smith, "Diffusion in catalyst pellets," Chem. Eng. Sci. **17**, 825–834 (1962).
[112]A. F. Olea and J. K. Thomas, "Rate constants for reactions in viscous media: Correlation between the viscosity of the solvent and the rate constant of the diffusion-controlled reactions," J. Am. Chem. Soc. **110**, 4494–4502 (1988).
[113]H. Wang and S. Torquato, "Dynamic measure of hyperuniformity and nonhyperuniformity in heterogeneous media via the diffusion spreadability," Phys. Rev. Appl. **17**, 034022 (2022).
[114]R. S. Langer and N. A. Peppas, Biomaterials **2**, 201–214 (1981).
[115]H. Wang, *PairFunctions Github repository* (GitHub, 2023).

31 January 2024 15:02:42

Published under an exclusive license by AIP Publishing